

Erlend Rysstad Mosbron

Evaluation of the Hot-Spot Method for a Bracket Geometry

Master's thesis in Subsea Technology

Supervisor: Sigmund Kyrre Ås

Co-supervisor: Arve Flesche

June 2022

NTNU
Norwegian University of Science and Technology
Faculty of Engineering
Department of Marine Technology



Norwegian University of
Science and Technology

Erlend Rysstad Mosbron

Evaluation of the Hot-Spot Method for a Bracket Geometry

Master's thesis in Subsea Technology
Supervisor: Sigmund Kyrre Ås
Co-supervisor: Arve Flesche
June 2022

Norwegian University of Science and Technology
Faculty of Engineering
Department of Marine Technology

Abstract

An important aspect in mechanical design is to assess the fatigue life of a component. A method for assessing fatigue is the hot-spot stress method, which involves computing the hot-spot stress at the weld toe. Using this method, complex structures can be analysed using the finite element method, often based on shell elements. There exists uncertainty with more complex plate geometries, such as brackets. Finite element analysis is performed on a specific bracket geometry, which is modelled using both solid and shell elements. Then, a manufactured specimen is tested. The hot-spot stresses at the weld toes of the bracket is extrapolated using strain gauges. The same specimen is then subjected to cyclic loads until fatigue failure is achieved. The hot-spot stresses for the same load range is compared with the S-N diagram for class D, according to the hot-spot method. It is found that the hot-spot stresses predicts failure, which indicates that the method is correct in this case. The stress range and cycles until failure found in the fatigue test is also compared to the relevant S-N diagram, to find which detail class align most with it, and thereby finding which detail class would give conservative prediction of fatigue life. In both these findings the number of tests were not sufficient to make any firm conclusions.

Sammendrag

Et viktig del ved mekanisk design er å vurdere utmattingslevetid hos en komponent. En slik metode er hot-spot spenningsmetoden, som innebærer å beregne hot-spot spenningen ved sveisetåen. Ved å bruke denne metoden kan komplekse strukturer analyseres ved hjelp av elementmetoden, ofte basert på skallelementer. Det er knyttet en del usikkerhet omkring komplekse plategeometrier, for eksempel braketter. Elementanalyse utføres på en spesifikk brakettgeometri, som er modellert ved bruk av både volum- og skallelementer. Deretter ble et prøvestykke, levert av Aker Solutions, testet under strekklast og utmatting. Først ble hot-spot spenningene ved sveisetåen til braketten ekstrapoleres ved hjelp av strekkklapper. Deretter ble prøven utsatt for sykliske belastninger, med en gitt spenningsvidde, inntil utmattingssvikt oppnås. Hot-spot spenningene, fra både elementanalysen og strekkklappene, sammenlignes med S-N-diagrammet for klasse D. Det ble vist ved hjelp av metoden, at det kom til å oppstå brudd, og dette tilsier at metoden er korrekt i dette tilfellet. Utmattingslevetid funnet i utmattingstesten sammenlignes også med det relevante S-N-diagrammet, for å finne hvilken klasse som stemmer best overens med prøvestykket, og derved finne hvilken klasse som ville gitt konservativ prediksjon av utmattelseslevetid. Antall tester var ikke tilstrekkelig til å gjøre noen sikre konklusjoner på resultatene.

Preface

This master's thesis is the result of work done at the Department of Marine Technology at the Norwegian University of Science and Technology (NTNU) during spring 2022. The work has consisted of reviewing literature, finite element analysis and material testing at the Marine Structures Laboratory.

The thesis was completed with the help and guidance of Associate Professor Sigmund Kyrre Ås. The thesis was proposed by Aker Solutions, and they provided the necessary test specimens.

Acknowledgements

I would like to express my gratitude to my supervisor, Sigmund Kyrre Ås, for guidance with the thesis, and for his eagerness to share his knowledge, especially regarding fatigue testing and FEA. I would also like to thank my co-supervisor at Aker Solutions, Arve Flesche, for his help and regular feedback during the process. Furthermore, I would like to thank Hjalmar Skarsvåg for his assistance with the experimental work in the laboratory, and especially for help with preparing the test specimen. Finally, I would like to thank Kenneth Njuolla for preparing the machines for testing and monitoring the results, and Kristian Minde for assisting with the testing rig.

Table of Contents

Abstract	i
Sammendrag	ii
Preface	iii
1 Introduction	1
1.1 Objectives	2
1.2 Outline	2
2 Background theory	4
2.1 Fatigue failure	4
2.2 Crack growth	5
2.3 Fatigue in welded structures	5
2.4 Cyclic loading	6
2.5 S-N diagram	7
2.6 Thickness correction	7
2.7 Assessment of fatigue	9
2.7.1 Nominal stress method	9
2.7.2 Hot-spot stress method	10
2.7.3 Notch stress method	11
3 Modeling and Finite Element Analysis	13
3.1 Creating the model	13
3.1.1 Creating the weld in the solid model	14
3.2 Symmetry and boundary conditions	14

3.2.1	Solid model	14
3.2.2	Shell model	15
3.3	Interaction between the two parts in each model	16
3.3.1	Solid model	16
3.3.2	Shell model	16
3.4	Applying the load	17
3.5	Applying the mesh	18
3.6	Inspecting the principal stresses in the models	19
3.6.1	Solid model	19
3.6.2	Shell model	20
3.7	Determining the hot-spot stresses	22
4	Experimental Setup and Procedure	24
4.1	Overview of test specimen	24
4.1.1	Grip section	24
4.1.2	Bracket section	25
4.1.3	Welding	26
4.2	Scanning the specimen	26
4.3	Static testing	27
4.3.1	Strain gauges	27
4.3.2	Data sampling	28
4.3.3	Test procedure	28
4.3.4	Obtaining stress values from the strain gauges	29
4.3.5	Extrapolating the hot-spot stresses	30
4.4	Fatigue testing	30
4.4.1	Calculations	31
4.4.2	Cross-sectional area	32
4.4.3	Long-life fatigue test	33
4.4.4	The second and final attempt	33
5	Results	35

5.1	The hot-spot stresses	35
5.1.1	Hot-spot stresses for the solid model	35
5.1.2	Hot-spot stresses from the shell model	36
5.1.3	Hot-spot stresses from the strain gauges	36
5.2	Evaluate the hot-spot method	37
5.3	The fatigue test	39
5.3.1	Fracture surface and crack initiation	41
6	Discussion	42
6.1	General remarks	42
6.1.1	Proportional relationship between load and stress	42
6.1.2	Scan of specimen	42
6.2	The hot-spot method	43
6.2.1	Comparing the solid and shell element	43
6.2.2	Comparing the different hot-spot stresses	43
6.2.3	Comparison of the stresses in the second specimen	44
6.3	The fatigue test	44
6.3.1	High load levels	45
6.4	Fracture surface	45
7	Conclusion and further work	46
7.1	Conclusion	46
7.2	Further Work	46
	Bibliography	48
A	Technical drawing of bracket toe	52
B	Weld geometry	55
B.1	Calculating the new weld geometry	55
C	Welding procedure specification	56
D	3D scan of specimen 1 using GOM Inspect	58

List of Figures

1.1	Example of a bracket used in a structure	1
1.2	Solid model and shell model of bracket	3
2.1	Illustration of cyclic stress with constant amplitude	6
2.2	S-N diagrams for steel in air (DNV-GL 2020)	8
2.3	Illustration of the two Hot Spot types (Lee et al. 2010)	10
2.4	Measurement of the hot spot strain range using linear extrapolation method (Erkki Niemi, Wolfgang Fricke, and Maddox 2018)	11
2.5	Modelling the effective notches at welds (Hobbacher 2016).	12
3.1	The geometry of the weld	14
3.2	Boundary conditions applied to the solid model	15
3.3	Boundary conditions applied to the shell model	15
3.4	The interaction between the two parts in the solid model	16
3.5	The interaction between the two parts in the shell model	17
3.6	Reference point and MPC constraints	18
3.7	Mesh applied to solid model	19
3.8	Mesh applied to shell model	19
3.9	A straight path from the weld toe	20
3.10	The stress distribution S22 in the shell model	21
3.11	Example: Determining stress at the weld toe	21
3.12	Hot spot stress at weld toe	23
4.1	Test specimen.	25
4.2	Specimen used to perform the tests.	25

4.3	Strain gauges mounted on the test specimen.	27
4.4	Graphic visualization of the application of loads (from first specimen). 28	
4.5	Calculating the stress from the strain gauges	29
4.6	Hot-spot extrapolation using strain gauges	30
4.7	Longitudinal attachment welded on the surface (DNV-GL 2020, p. 142). 32	
4.8	Cross section of the area under the weld toe.	32
5.1	Comparison of the hot-spot method in Abaqus an specimen 1	39
5.2	Comparison of the hot-spot method in Abaqus an specimen 2	39
5.3	Stress range	40
5.4	Stress range	40
5.5	Fracture surface of specimen subjected to fatigue failure	41
5.6	Initiation of crack on the opposite weld toe	41
B.1	Weld geometry for a 50 mm thick plate, provided by Aker Solutions .	55
D.1	3D scan - from the side	58
D.2	3D scan - from the top	59
E.1	Specimen 1 - Stress in strain gauge 1	60
E.2	Specimen 1 - Stress in strain gauge 2	61
E.3	Specimen 1 - Stress in strain gauge 3	61
E.4	Specimen 1- Stress in strain gauge 4	62
E.5	Specimen 1 - Stress in strain gauge 1 and 4	62
E.6	Specimen 1 - Stress in strain gauge 1 and 2	63
E.7	Specimen 1 - Stress in strain gauge 1, 2, 3 and 4	63
E.8	Specimen 2 - Stress in strain gauge 1	64
E.9	Specimen 2 - Stress in strain gauge 2	64
E.10	Specimen 2 - Stress in strain gauge 3	65
E.11	Specimen 2 - Stress in strain gauge 4	65
E.12	Specimen 2 - Stress in strain gauge 1 and 4	66
E.13	Specimen 2 - Stress in strain gauge 1 and 2	66

E.14 Specimen 2 - Stress in strain gauge 3 and 4	67
E.15 Specimen 2 - Stress in strain gauge 1, 2, 3 and 4	67

List of Tables

3.1	Linear-elastic material properties	13
3.2	The force applied to the models in the FEA	18
3.3	Location of stress values near the weld toe in the solid model	20
3.4	Stress values near the weld toe in the shell model	22
4.1	Excerpt from welding parameters	26
4.2	S-N curve for class E detail in air	32
4.3	The load levels for the first attempted fatigue test	33
4.4	The load and stress levels for the final fatigue test	34
5.1	The hot-spot stresses from the solid model	35
5.2	The hot-spot stresses from the shell model	36
5.3	The first specimen, strain gauge 1 and 2	36
5.4	The first specimen, strain gauge 3 and 4	37
5.5	The second specimen, strain gauge 1 and 2	37
5.6	The second specimen, strain gauge 3 and 4	37
5.7	The hot-spot stress corresponding to the load range	38

Chapter 1

Introduction

Fatigue failure is a highly relevant form of failure that needs to be accounted for in structures and other mechanical components. In offshore installations, it is crucial to design the different structural components to withstand the effects of cyclic loading, as these structures are exposed to large loads from both wind and waves throughout their lifespan. Fatigue cracks are prone to initiate at corners, as stresses have a tendency to concentrate at these points. Brackets have been implemented in corner points to redistribute the stress through the connection, and increase the fatigue life of the global structure (Irving et al. 2005).



Figure 1.1: Example of a bracket used in a structure

The brackets are typically joined by welding. Fatigue cracks have a higher likelihood of developing in welds, and therefore it is necessary to assess the fatigue life in these regions (Dieter Radaj 1990). Finite element analysis of the structures is performed by computing the hot-spot stress at the weld toe, which is used to predict the fatigue life.

In most cases, structures are modeled using shell elements, as this is a simple process which produces a conservative estimate of the hot-spot stress. In comparison, solid models are more time consuming for complex structures. However, as there exists considerable uncertainty regarding how the shell model should be constructed to produce accurate hot-spot stresses near brackets, assessing the fatigue at these points can be a challenge.

1.1 Objectives

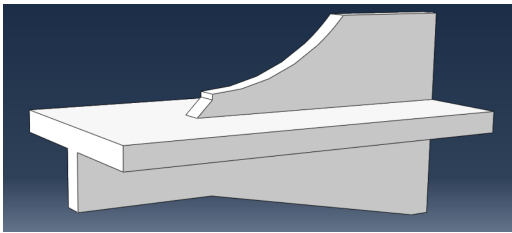
The objective of this thesis is to evaluate the hot-spot method for bracket geometries. A test specimen with a bracket geometry, provided by Aker Solutions, is considered. Finite element analysis is performed based on solid and shell models of the specimen, and this is used to assess fatigue life using the hot-spot method. Then the same method is applied to the test specimen, by recording the stresses resulting from static loads, using strain gauges at the hot-spot extrapolation points. and fatigue test were the specimen are subjected to cyclic loads at different stress ranges to achieve failure, which gives a stress range and cycles until failure, which can be compared to the results from the hot-spot method.

1.2 Outline

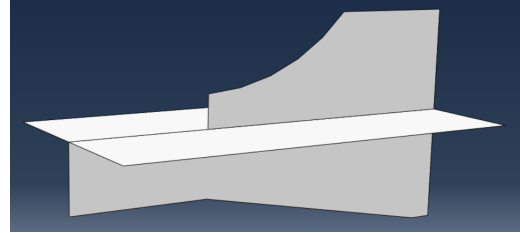
An overview of the theory regarding fatigue, fatigue testing and finite element analysis is presented in chapter 2. Sections from this chapter are more or less taken directly from the pre-project conducted during the autumn of 2021 [7]. The procedure for performing the finite element analysis, together with theoretical



(a) Bracket in test specimen



(b) Model based on solid elements



(c) Model based on shell elements

Figure 1.2: Solid model and shell model of bracket

justification, is presented in chapter 3. Thereafter follows the setup and procedure for laboratory testing in chapter 4. These two chapters constitutes the methodology of the thesis. The results from the different tests are processed and presented in chapter 5. The obtained results are discussed in chapter 6. Concluding remarks are given in chapter 7, and recommendations for further work concludes the thesis.

Chapter 2

Background theory

The following chapter provides the theoretical background of the finite element analysis and experimental work in the succeeding chapters, which includes an introduction to the key aspects of fatigue failure and fatigue assessment methods. The content is based on the specialisation project written in preparation for thesis.

2.1 Fatigue failure

Repetitive or cyclic loads applied to a component can result in physical damage of the material, and is referred to as fatigue (Dowling 2013). The resulting cyclic stresses can cause cracks to develop and grow until structural failure. Fatigue failures can occur at stress levels below the ultimate strength of the material, and even within the yield strength (Suresh 1998). It is common to separate between high cycle fatigue and low cycle fatigue. High cycle fatigue is traditionally concerned with failures that require more than 10^4 cycles to experience failure, while low cycle fatigue is concerned with failure that occurs due to higher stress levels and the occurrence of plastic deformation (Lotsberg 2016).

2.2 Crack growth

The fatigue life may be divided into three stages.

- Crack initiation
- Crack propagation
- Final failure

The distinctions, in real life, between the first two stages are not easy to define (Suresh 1998). During the first phase, the cyclic load causes microscopic imperfections in the material to grow into macroscopic cracks (Antaki and Gilada 2015). The next phase is characterized by crack growth, and it is now possible to estimate the fatigue life. The crack continues to grow due to the cyclic loads, and eventually this results in the structural failure of the component.

2.3 Fatigue in welded structures

As mentioned above, the crack may also initiate at existing internal or surface cracks. In a welded structure that is subjected to a fatigue loading, the fatigue life is strongly dependent on the welded joint, as failure most likely originates from this location (Dieter Radaaj 1990). There is a total of four different failure modes that should be considered when assessing the possibility of fatigue failure in the weld, and crack growth from the weld toe into base material is the most frequent (Lotsberg 2016). The weld toe is typically a point with high, local stress concentration, due to the presence of welding defects, such as lack of penetration and undercuts (E. Niemi 1995). Other reasons might include an uneven toe shape, and residual stresses from the welding process (Mikkola, Murakami, and Marquis 2014).

2.4 Cyclic loading

Materials which experience fatigue is subjected to loads that cycle between high and low levels. With regards to controlled fatigue tests, the load cycle is often described with a constant amplitude and a constant mean load. A sinusoidal function is typically used to describe the application of load over time(Berge and Ås 2017). The resulting stress levels are illustrated in Figure 2.1.

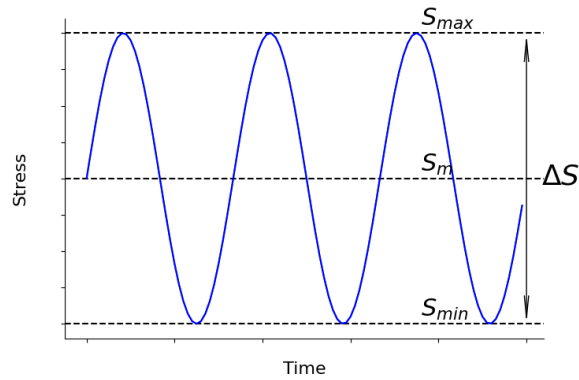


Figure 2.1: Illustration of cyclic stress with constant amplitude

S_{max} is the maximum stress level

S_{min} is the minimum stress level

S_m is the mean stress level

ΔS is the stress range

From these parameters, it is possible to introduce the stress ratio R , which is sometimes referred to as the R-ratio. It is defined as the ratio of the lowest stress to the highest stress in a loading cycle:

$$R = \frac{S_{min}}{S_{max}} \quad (2.1)$$

Furthermore, the following relationship between the mean stress S_m , stress range ΔS and stress ratio R (Berge and Ås 2017):

$$S_m = \frac{\Delta S}{2} \left(\frac{1 + R}{1 - R} \right) \quad (2.2)$$

2.5 S-N diagram

If a test specimen of a material is subjected to a level of cyclic stress, a fatigue crack will develop until final failure after a certain number of cycles. Testing the same specimen at a higher stress level, the number of cycles to failure will be smaller (Dowling 2013). By repeating the test for different stress ranges, the stress ranges ΔS and number of cycles to failure, denoted as N , is plotted in a log-log diagram. From these scattered values it is possible to create a mean S-N diagram based on linear regression analysis (Lotsberg 2016). The mean diagram is linked with 50% survival probability, and is used to find the regression constant for the slope (Berge and Ås 2017). From this regression constant, $\log a$, it is possible to compute the constant $\log \bar{a}$, a slope two standard deviations below the mean:

$$\log \bar{a} = \log a - 2s_{\log N} \quad (2.3)$$

where $s_{\log N}$ is the standard deviation of $\log N$. Finally, according to DNV-GL 2020, the basic design S-N curve is given in Equation 2.4 and is associated with 97.7% probability of survival.

$$\log N = \log \bar{a} - m \log \Delta S \quad (2.4)$$

The design S-N diagram serves as an important basis for fatigue design. The inputs $\log \bar{a}$ and m are based on joint classifications, which are provided in appendix A of DNV-GL 2020. S-N diagrams for steel in air, based on Equation 2.4, is included in Figure 2.2.

2.6 Thickness correction

The thickness of a specimen is found to have an impact on the fatigue life. Increasing the thickness of a given type of fatigue specimen while retaining all the other parameters, will in general cause a decrease in fatigue strength (Berge 1985). For welded connections that are larger than the reference thickness $t_{ref} = 25 \text{ mm}$,

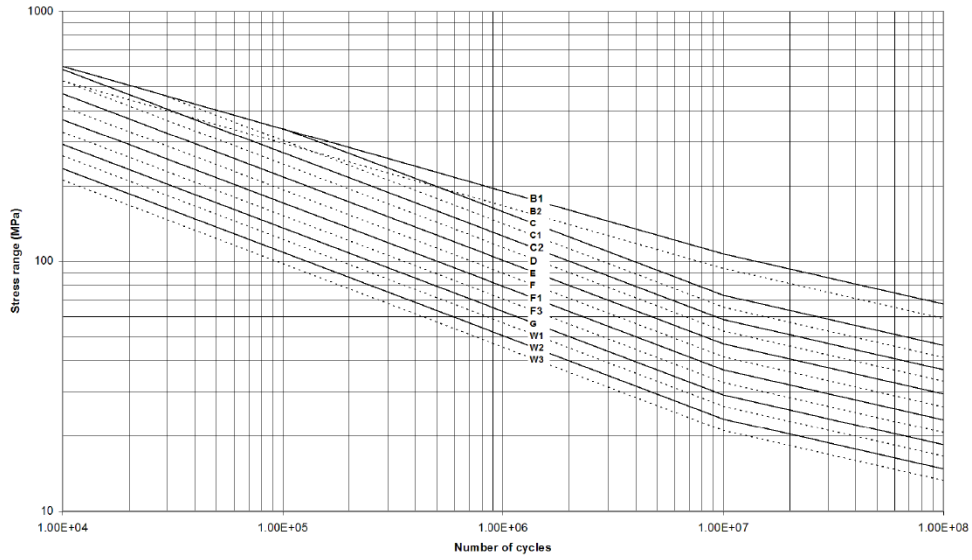


Figure 2.2: S-N diagrams for steel in air (DNV-GL 2020)

a thickness correction is introduced by a modification of the stress range ΔS_{ref} .

$$\Delta S_{ref} = \Delta S \left(\frac{t}{t_{ref}} \right)^k \quad (2.5)$$

There is a tendency for thin plates, with thickness $t \leq t_{ref}$, to have increased fatigue life (Berge and Ås 2017, p. 154). Nevertheless, it is not advisable to use the thickness effect to increase the fatigue life of the specimen.

2.7 Assessment of fatigue

Fatigue is an important failure mode to consider when designing mechanical components or structures. The fatigue life may be affected by various factors, such as material properties, the geometry of the component, load conditions, the environment or temperature (Achintha et al. 2014). However, fatigue is considered a fairly unpredictable process, and in many cases it is difficult to accurately determine and model every aspect which is going to affect the component during its entire lifetime. Fatigue analysis involves determining whether or not the cyclic stresses in the material will lead to structural failure, and in that case determine how many of the cycles until failure the material can withstand. Mechanical design against fatigue can ensure that the material has a suitable lifespan.

Fatigue analysis is performed in the high cycle region where stress is relatively low and deformation is primarily elastic. "Fatigue design of offshore steel structures", a standard established by DNV-GL 2020 is a recommended practice in relation to fatigue assessment.

2.7.1 Nominal stress method

Nominal stress is described as the average stress over a given cross-section, and can be derived from classical beam theory or finite element analysis. Traditional fatigue analysis of welded components is based on the use of nominal stress S-N curves, which corresponds to a certain geometry and load configuration (Hobbacher 2016). Fatigue life is determined by comparing the detail of the weld with the S-N diagram given in standards, such as in appendix A of DNV-GL 2020. In the nominal stress approach, This method is only applicable if the joint under consideration is geometrically simple. Detail dimensions, welding methods and other parameters will vary in different weld joints, and therefore this method is not necessarily applicable in more complex cases (Hobbacher 2016).

2.7.2 Hot-spot stress method

More recently, the hot-spot stress method has been used as an alternative to the nominal stress method when designing welded plate structures. The hot-spot is defined as the region where the crack is expected to initiate. This could for instance be at the weld toe, because to the large stress concentration and the geometry of the weld or a similar notch (DNV-GL 2020). The approach is based on the stress range of the spot hot-spot stress, which can be referred to as hot-spot stress range. The hot-spot stress, also called structural stress, is a combination of membrane stresses and bending stresses. (DNV-GL 2020). One advantage of the hot-spot stress approach compared to the nominal stress approach is that complex geometries can be analysed (Mecséri and Kövesdi 2020).

Hot spots can be classified in mainly two ways (Erkki Niemi, Wolfgang Fricke, and Maddox 2018). For type "A", the weld toe is located on a plate surface, while for type "B", the weld toe is located on a plate edge. In this thesis, mainly type "A" is considered.

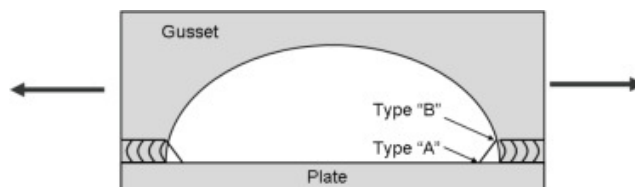


Figure 2.3: Illustration of the two Hot Spot types (Lee et al. 2010)

The structural hot-spot stress may be determined using strain gauges. Two strain gauges are placed ahead of the weld toe, as denoted by ε_A and ε_B , as shown in Figure 2.4. The points are located at different places according to different standards, but common among them is that they are often expressed as a function of the thickness t . The assumption made is that the strain, and subsequently the stresses, in the element increases linearly in the direction of the weld toe, and one is therefore able to estimate the hot-spot stress using linear extrapolation (D. Radaaj, Sonsino, and W. Fricke 2009).

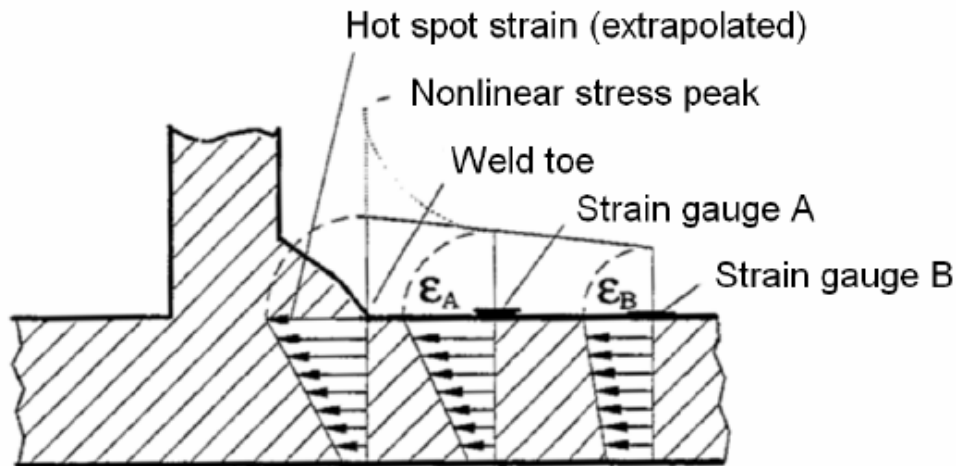


Figure 2.4: Measurement of the hot spot strain range using linear extrapolation method (Erkki Niemi, Wolfgang Fricke, and Maddox 2018)

DNV-GL 2020 has recommended two methods, A and B, for derivation of hot-spot stress. For method A, a linear extrapolation of the stresses to the intersection line from the read out points at $0.5t$ and $1.5t$ from the intersection line or weld toe, corresponding to shell and solid models respectively, can be performed to derive hot-spot stress. Assessment of fatigue strength is in general done by comparing the effective hot-spot stress with the D-curve.

2.7.3 Notch stress method

There are still some geometries that are difficult to analyze with the hot-spot stress using this approach. The notch stress approach has been developed, which is recommended to and works well independent of the geometry of the joint. Assuming linear-elastic behaviour, the notch stress is defined as the total stress at the weld toe or root. The approach involves replacing the real weld with an "effective weld" at the locations that are depicted in Figure 2.5(DNV-GL 2020). As shown in the figure, the notches may be introduced in the weld toes or at the weld roots. The reference radius ρ_f takes account of the statistical nature and

scatter of weld shape parameters, as well as of nonlinear material behaviour at the notch root (Sonsino et al. 2012). For structural steels, an effective notch root radius of $\rho_f = 1.0\text{mm}$ has been verified to give consistent results. The method is limited to thicknesses $t \geq 5\text{mm}$, since the method has not yet been verified for smaller wall thicknesses (Hobbacher 2016).

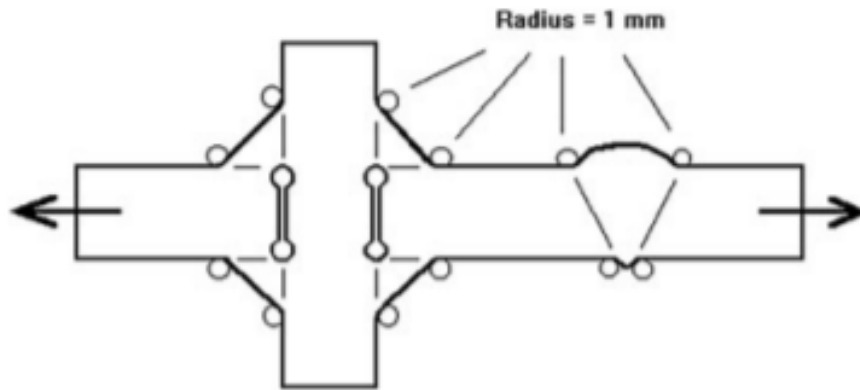


Figure 2.5: Modelling the effective notches at welds (Hobbacher 2016).

The results of this method are more accurate in comparison to the hot-spot stress approach, and represents fatigue life better by including local geometrical effects with the implementation of the reference radius (Ringsberg et al. 2014). The notch stress approach is also used for analysing fatigue crack initiating from the weld toe (Wolfgang Fricke 2008). Disadvantages to this approach is that for more complex weld joints, it may require more effort to create the model. Especially the area around the region of the notch can be detailed and time-consuming. It may also prove necessary to apply a higher mesh density in the region around the notch, which would increase the computational time in comparison with the hot-spot method.

Chapter 3

Modeling and Finite Element Analysis

The purpose of this chapter is to give a description of the modeling and finite element analysis performed during the course of the project. This includes an overview of the solid and shell model, and the method for extrapolating the hot-spot in each case. The specimens were modeled in Solidworks and Abaqus, while the analysis was performed solely in Abaqus.

3.1 Creating the model

The solid and shell model were produced according to the mechanical drawing in Appendix A. When creating the shell model, the geometry of bracket section is based on the middle surface in the plates, and the shell thickness is defined as 8. The material properties that were used is provided in Table 3.1.

Table 3.1: Linear-elastic material properties

Young's modulus	210000 <i>MPa</i>
Poisson's ration	0.3

3.1.1 Creating the weld in the solid model

One difference between the solid and shell model, is that the solid model is recommended to include the geometry of the weld. The weld was modeled according to the figure and calculations in Appendix B, which resulted in the dimensions shown in Figure 3.1. This is an idealised geometry, and does not have this shape in real life, as seen in Figure D.1.

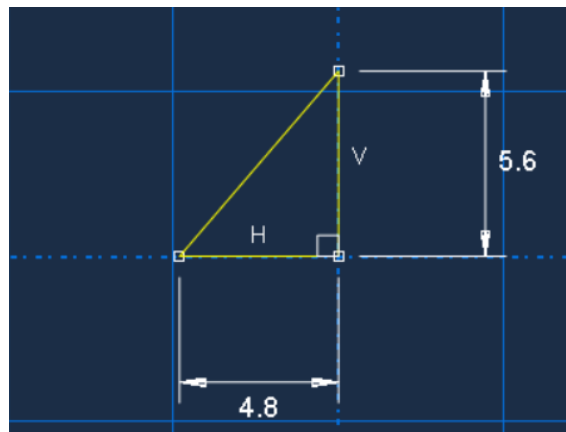


Figure 3.1: The geometry of the weld

3.2 Symmetry and boundary conditions

By taking advantage of the symmetry that of the specimen, it was possible to simplify the models that were used in the analysis.

3.2.1 Solid model

When creating the solid model from the specimen, the total volume of the model was reduced to a quarter of a full size model. This reduces the number of total solid elements in the mesh and subsequently the computation time needed to perform the analysis is decreased. The symmetry boundary condition is applied to the two surfaces, as shown in Figure 3.2. Due to the orientation of the model, this means symmetry about the XY- and XZ-plane, introducing the following restraints on

translation U and rotation R :

$$U_z = 0 \quad R_x = 0 \quad R_y = 0$$

$$U_y = 0 \quad R_x = 0 \quad R_z = 0$$

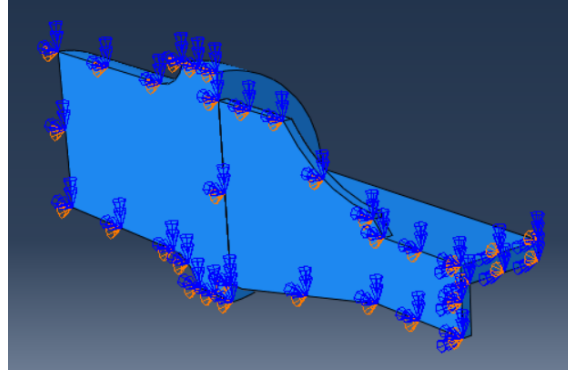


Figure 3.2: Boundary conditions applied to the solid model

3.2.2 Shell model

The symmetry is taken into account, and the model is split across the middle of the test specimen. This boundary condition is applied to the shell edge as shown in Figure 3.3, creating symmetry about the XY plane.

$$U_z = 0 \quad R_x = 0 \quad R_y = 0$$

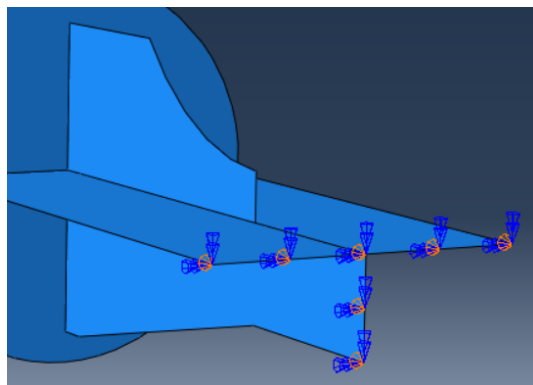


Figure 3.3: Boundary conditions applied to the shell model

3.3 Interaction between the two parts in each model

In both models it was also decided to create the grip section and the bracket section as separate parts. The main reason for this was that the grip section could be used for both the solid and shell model of the bracket, but it also proved to simplify the process of applying the mesh.

3.3.1 Solid model

In the solid model, the two parts are connected using the "Tie constraint". This is chosen to be a surface-to-surface connection, where the bracket section acts as the master and the grip section acts as the slave, as can be seen in Figure 3.4. The tie constraint is based on connecting the nodes that are close together, so that translation and rotation of the nodes are identical (Dassault Systèmes 2008).

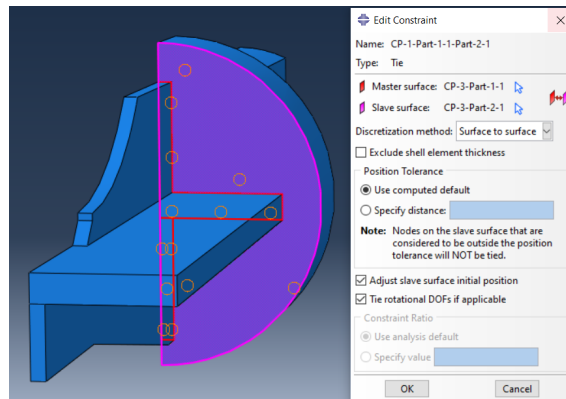


Figure 3.4: The interaction between the two parts in the solid model

3.3.2 Shell model

In the shell model, the two parts are connected using the "Shell-to-solid" couplings. The shell edges that connect to the surface of the grip section are specified in Abaqus, as shown in Figure 3.5. The "Shell-to-solid" coupling consists of an internal set of constraints that distributes translation and rotation from the nodes on the shell edge onto the nodes on the solid surface. For each shell node involved in the coupling,

a distinct internal distributing coupling constraint is created where the shell node acts as the reference node and the nearby solid nodes acting as the coupling nodes. This means that the forces and moments will be distributed evenly on the related solid nodes that acts as coupling nodes, and one result of this is continuous stress between the elements (Dassault Systèmes 2008).

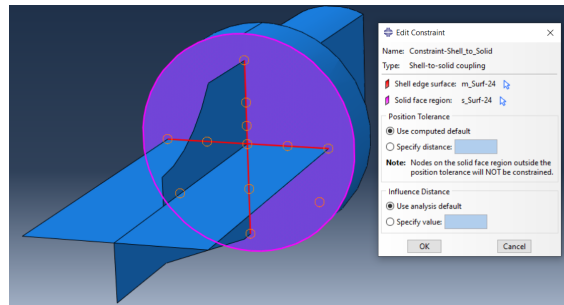


Figure 3.5: The interaction between the two parts in the shell model

3.4 Applying the load

Under "Step", the loading is defined as a "Static, General". The load was applied on the grip section of the models, where the clamps of the test rig are fixed. In Abaqus, the most relevant static loading for applying a load magnitude on a specimen is the "Concentrated force". As this force is applied to one node, one way to correct this is to constrain the surface on the end of the specimen to a point in the centre of the surface. This is done by first creating a "Reference Point". This point is in the same location for both the solid and shell model, and is shown in Figure 3.6. Then the multi-point constraint (MPC) is used to connect the displacement of the surface of a region to the displacement of a single point, which in this case is the reference point (Dassault Systèmes 2008).

Now it is possible to apply a "Concentrated force" to the previously created point, directing the force away from the assembly to simulate tension. The models were subjected to the same load magnitudes as were applied to specimen during the static testing in the laboratory, as described in subsection 4.3.3. Due to the solid model

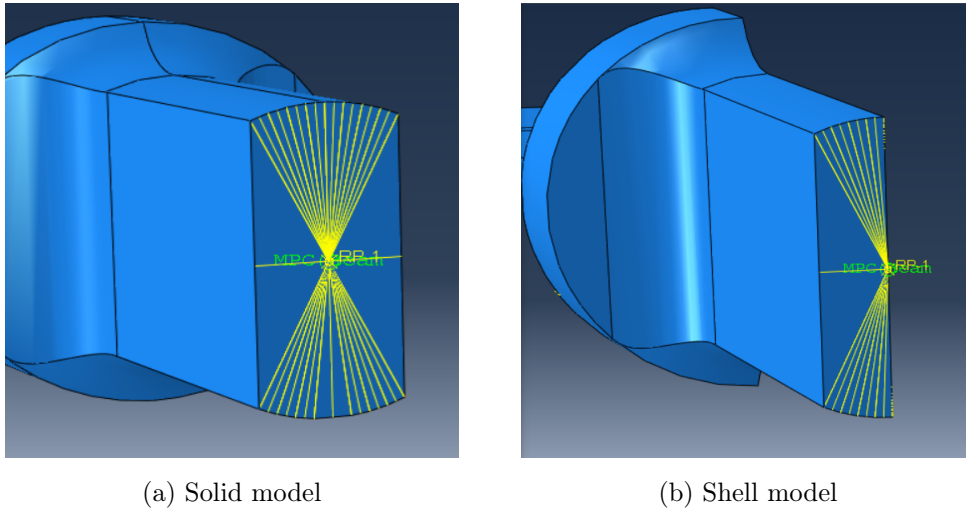


Figure 3.6: Reference point and MPC constraints

being half the size of the shell model, the force magnitude that is applied to the solid model is divided by two. The loading levels are presented in Table 3.2

Table 3.2: The force applied to the models in the FEA

Solid model	Shell model
1000 N	2000 N
2500 N	5000 N
5000 N	10000 N

3.5 Applying the mesh

The global size of the elements in the mesh were set to 8 mm . The bracket consists of hex shaped elements, and element type 20-node quadratic, solid elements with reduced integration, denoted C3D20R. Measures were taken to ensure an even distribution of elements, and the final model with mesh is included in Figure 3.7.

The global size of the elements in the mesh were set to 8 mm . The element shape is defined as quad, and the element type is S8R, an 8-node doubly curved thick

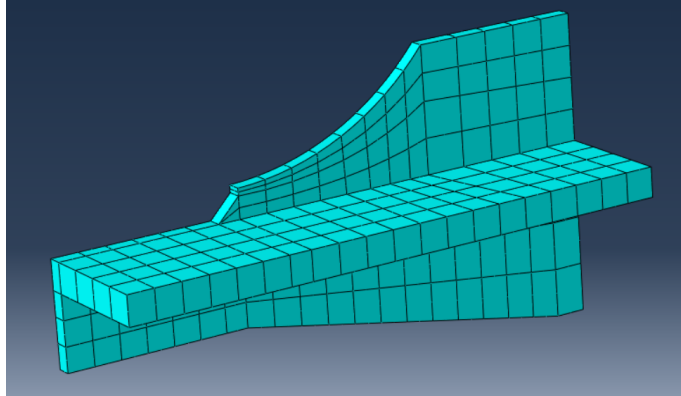


Figure 3.7: Mesh applied to solid model

shell, with reduced integration. Measures were taken to ensure a even distribution of elements, and the final model with mesh is shown in Figure 3.8.

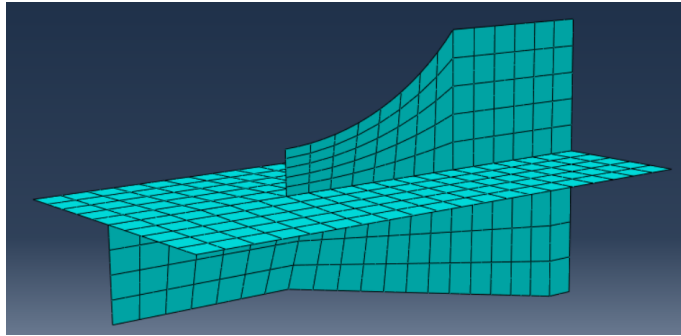


Figure 3.8: Mesh applied to shell model

3.6 Inspecting the principal stresses in the models

After running the analysis, the stresses that are oriented in the same direction as the applied force were inspected. In the present case, this corresponds to the stress component S22 in Abaqus. It is not possible to read the stresses at the hot-spot extrapolation points directly, so the values are approximated.

3.6.1 Solid model

A path is created from the weld toe, as shown in Figure 3.9.

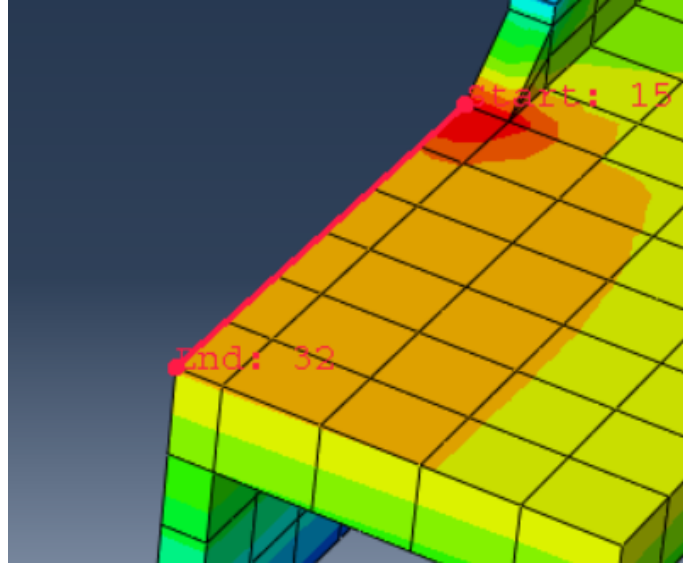


Figure 3.9: A straight path from the weld toe

The locations of the corner nodes of the elements along this path is then presented in Table 3.3.

Table 3.3: Location of stress values near the weld toe in the solid model

Distance from weld toe [mm]
0
7.33334
14.6667

3.6.2 Shell model

The stress distribution in the shell model is different depending on which surface of the shell elements are observed. In Abaqus, this is selected under Results → Field Output → Section Points. The difference is clearly observed in Figure 3.10. The stresses displayed at (b) Top is the stresses at the plate surface, as verified by the solid element stress solution.

Extrapolating the stresses turned out to be a challenge. Contrary to the solid

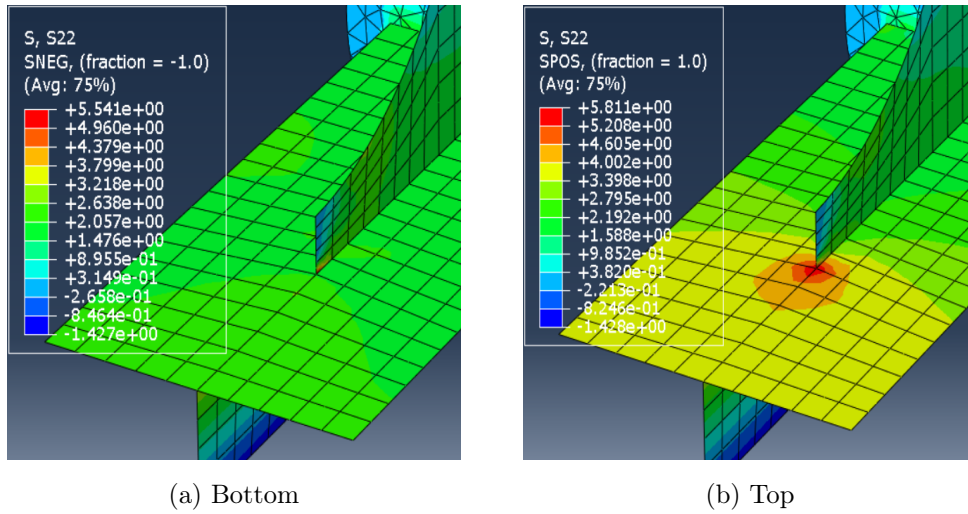


Figure 3.10: The stress distribution S22 in the shell model

elements, it is not possible to plot the stresses along a path, as it is to distinguish the nodes of a specific shell from the nodes of the connecting element. This was the case with the bracket. The solution was to examine the element nodes along the path from the weld toe individually, and manually read out the stresses in the locations that were necessary to determine the hot-spot extrapolation points. The shell elements consists of 8 nodes, and so when examining four elements which all share one corner, the value that repeats in every case is the corner node. For example, the stress at the weld toe is determined in Figure 3.11

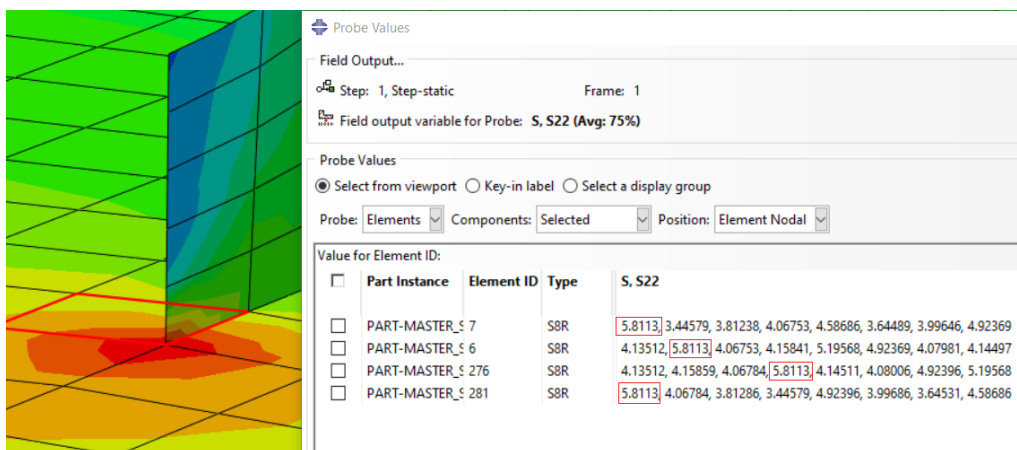


Figure 3.11: Example: Determining stress at the weld toe

The stresses in the corner nodes of the elements along this path is then presented

in Table 3.4.

Table 3.4: Stress values near the weld toe in the shell model

Distance from weld toe [<i>mm</i>]
0
8.33334
16.6667

3.7 Determining the hot-spot stresses

As previously mentioned, the hot-spot extrapolation points are located at distances $0.5t$ and $1.5t$ from the weld toe. This corresponds to the locations 4 mm and 8 mm from the weld toes of the models. To find the stress values at these points, a simple python script was written which used the "Polyfit" function from Numpy. This method is based on the least squares method within regression analysis, and gives an approximation of the stresses. The best fit was achieved with a quadratic function. From the hot-spot extrapolation points, linear extrapolation is performed to create a straight line that goes through these points and gives a hot-spot stress value at the weld toe. The method is illustrated in Figure 3.12

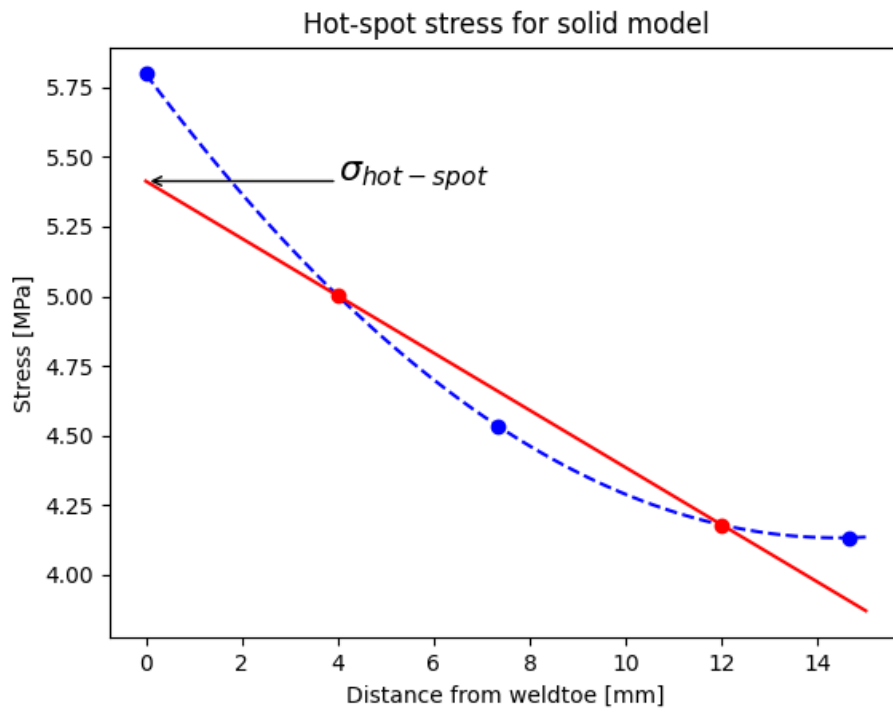


Figure 3.12: Hot spot stress at weld toe

Chapter 4

Experimental Setup and Procedure

The purpose of this chapter is to give a description of the preparation and execution of the laboratory testings. This includes an overview of the test specimen, The experimental tests were conducted in the laboratory of the Department of Marine Technology, NTNU. Static tests were performed to obtain the stresses at the hot-spot extrapolation points, so that these could be compared with results from FEA. Dynamic tests would give information on fatigue life.

4.1 Overview of test specimen

The four specimens were provided by Aker Solutions AS. It is assumed that the test specimens are manufactured from high strength steel of grade VL A36 or similar, as defined by DNV-GL 2019. The test specimen are produced in accordance to the technical drawing found in Appendix A.

4.1.1 Grip section

The grip section is shown on each end of the specimen in Figure 4.1 and close-up in Figure 4.2. The transition between these segments was planned to be rounded, with a radius of $r = 20 \text{ mm}$ to reduce stress concentrations in the area, but due to complications in the manufacturing process, this transition is closer to a 45-degree angle. In all the four specimen which are tested, this section has been machined



Figure 4.1: Test specimen.

from a single part.

4.1.2 Bracket section

There are two brackets in the specimen to provide symmetry. The plate fixed opposite of the bracket, as shown in 4.2, represents a girder. It was originally intended for the girder to have a uniform height, but the final model included a slope under the bracket, reducing the height in the middle of the specimen. The results were an reduction in the stresses at the angle between the girder and cylindrical part. The smaller cross-sectional area also lead to more evenly distributed stresses in this region.



Figure 4.2: Specimen used to perform the tests.

4.1.3 Welding

The different parts were welded together according to the welding procedure specification (WPS) as included in Appendix C. The edges of the plates, where the weld bead would be laid, are beveled to a V-shaped groove to ensure full penetration and fusion of the materials. Prior to welding, the separate plates were fixed to minimize heat distortion of the final product. The welding was performed according to welding process 136, which denotes tubular cored metal arc welding with active gas shield (Leonard P. Connor 1991). The filler metal corresponds to the classification "AWS A5.36 E81T9-M21A8". Selected welding parameters, for the given filler metal and plate thickness $t > 7$, is provided in Table 4.1.

Table 4.1: Excerpt from welding parameters

Diameter [mm]	Wire feed speed [m/min]	Current [A]	Voltage [V]	Current -	Welding speed [mm/min]
1,20	6,00 - 8,00	180 - 240	21,0 - 24,0	DC+	130 - 275
1,20	7,00 - 11,0	220 - 290	22,0 - 25,0	DC+	280 - 550
1,00	6,00 - 11,0	130 - 220	19,0 - 23,0	DC+	120 - 320

4.2 Scanning the specimen

The specimen were scanned using GOM Inspect, which allowed for inspecting a 3D-model of the specimen using the software. The main purpose of this was to see if the specimen was distorted, and would be subjected to undesirable bending moment. This was done by comparing the scanned model with the solid model constructed using CAD. The 3D-scan of the first specimen is included in Appendix D, where the colours and plotted labels indicate misalignment compared to the solid model. It does not seem to be indications of considerable misalignment which would result in bending.

4.3 Static testing

The static tests were performed using INSTRON model 1342, a servo-hydraulic test apparatus which has a maximum load capacity of 100 kN . The tests were conducted at room temperature.

4.3.1 Strain gauges

The strain was measured using strain gauges. Since the specimen is relatively small and it was desirable to measure the strain at exact points, it was determined to select among the stain gauges with the lowest gauge length. Furthermore, it was only necessary to measure the strain fields in one direction, and therefore uniaxial strain gauges were sufficient. For the first specimen, the model FLA-1-11-3L from TML was used, for the second specimen, the model 1-LY13-1/350ze from HBM was used.



Figure 4.3: Strain gauges mounted on the test specimen.

According to DNV-GL 2020, the stress read-out points to extrapolate the hot-spot stress are located at distances $0.5t$ and $1.5t$ from the weld toe. For this specimen, with thickness $t = 8\text{ mm}$, this corresponds to 4 mm and 12 mm . However, these are placed 4 mm and 16 mm from the weld toes. There where placed four strain gauges on the specimen, which each are designated a number from 1 to 4, as shown in Figure 4.3. Therefore, it was possible to extrapolate the hot-spot stresses at both

weld toes.

4.3.2 Data sampling

A HBM QuantumX MX1615B is used to collect the data from the strain gauges. This is a universal data acquisition system that is well suited for the job. The software used to capture the data is CatmanAP, a software made by HBM. This software was used for calibrating, storing and processing the resulting data.

4.3.3 Test procedure

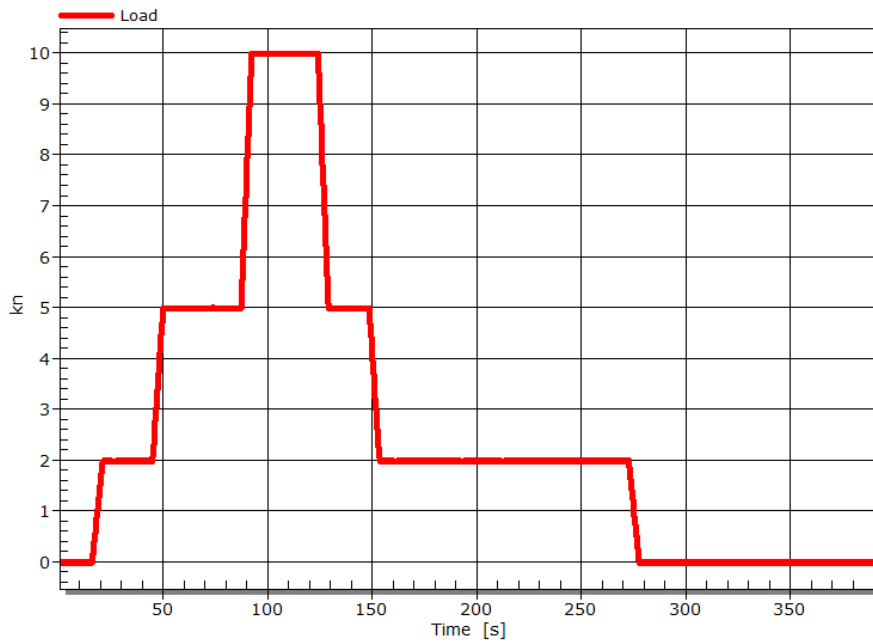


Figure 4.4: Graphic visualization of the application of loads (from first specimen).

The specimen were subjected to static, tensile loads of magnitude 2 kN , 5 kN and 10 kN . It was confirmed that the registered strain acted proportionally to the applied load. The tests were conducted by applying the loads in ascending order, and then in descending order, as shown in Figure 4.4. Each load was maintained for at least 10 seconds, and it took five seconds to increase or reduce the load to a

new level. For each specimen, loading was performed several times prior to recording the results.

4.3.4 Obtaining stress values from the strain gauges

In the elastic region of the material, there exists a linear relationship between the strains ε and stresses σ . This linear-elastic behaviour is described mathematically by Hooke's law:

$$\sigma = E\varepsilon \quad (4.1)$$

From this relationship it is simple to calculate the stress that acts in the location of the four strain gauges. This is done using the in-built function "Strain gauge stress analysis" in CatmanAP, after providing the relevant material properties. For example, the stresses from the first strain gauge (SG1) is computed in Figure 4.5.

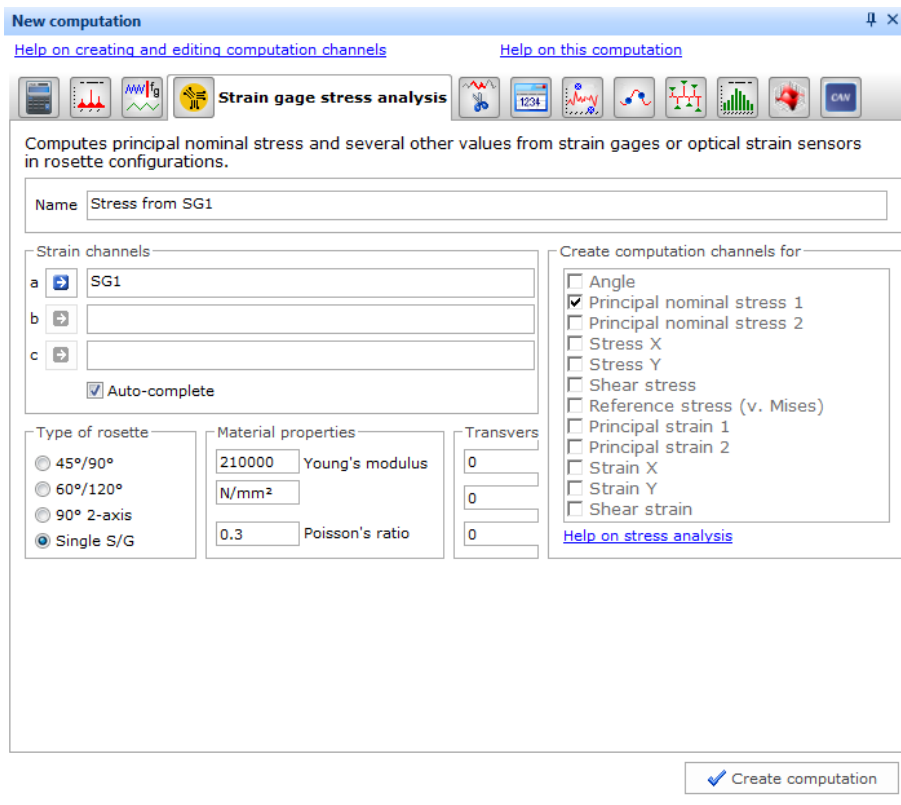


Figure 4.5: Calculating the stress from the strain gauges

4.3.5 Extrapolating the hot-spot stresses

The hot-spot stresses were calculated at both weld toes using the stress values from the corresponding strain gauges. The linear extrapolation method was applied to create a line that went through the stress values and gives a hot-spot stress value at the weld toe. The method is illustrated in Figure 4.6, using the readings from strain gauge 1 and 2 in the first specimen as an example. The results are presented in subsection 5.1.3.

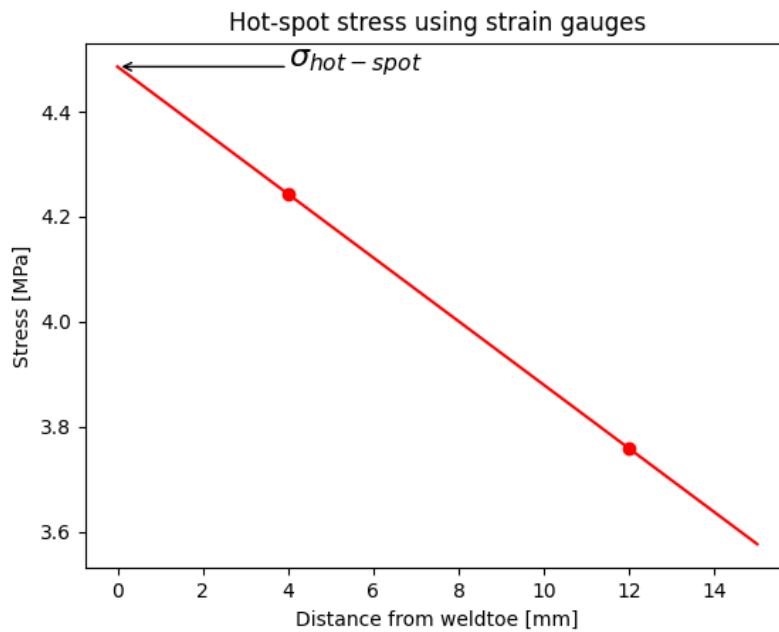


Figure 4.6: Hot-spot extrapolation using strain gauges

The results are presented in subsection 5.1.3.

4.4 Fatigue testing

The final dynamic test was performed by a testing rig with maximum load capacity of 2000 kN . The fatigue test was performed with a frequency of $f = 2.6\text{ Hz}$. The tests were conducted at room temperature.

4.4.1 Calculations

Prior to executing the fatigue testing, it was necessary to establish the loading cycles.

The general design SN-curve is found in DNV-GL 2020:

$$\log N = \log \bar{a} - m \log \Delta S \quad (4.2)$$

Equation 4.2 is rearranged with respect to $\log \Delta S$

$$\log \Delta S = \frac{\log \bar{a} - \log N}{m_1} \quad (4.3)$$

The stress range ΔS is then determined

$$\Delta S = 10^{\log \Delta S} \quad (4.4)$$

The mean stress S_m is found using the relationship

$$S_m = \frac{\Delta S}{2} \cdot \frac{(1 + R)}{(1 - R)} \quad (4.5)$$

where R is the stress-ratio that the tests will be conducted under. Now the maximum and minimum stress values, S_{max} and S_{min} , can be determined

$$S_{max} = S_m + \frac{\Delta S}{2} \quad S_{min} = S_m - \frac{\Delta S}{2} \quad (4.6)$$

Finally, the corresponding load levels F_{max} and F_{min} is found using the cross-sectional area A

$$F_{max} = S_{max} \cdot A \quad F_{min} = S_{min} \cdot A \quad (4.7)$$

Classification of the geometrical detail

The bracket is welded on the surface of a plate that is stressed in the longitudinal direction. The weld toe is located at the end of the bracket, and is consequently transverse to the stress direction. It is reasonable to assume that the crack will initiate at the weld toe on the stressed surface, as illustrated in Figure 4.7. For the following calculations, this geometry is assumed to be a class E detail, according to attachment A in DNV-GL 2020. The S-N curve, and the constants $\log \bar{a}$ and m_1 , is defined in Table 4.2.

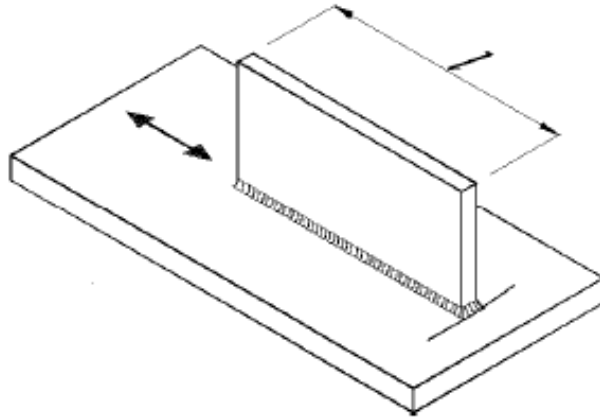


Figure 4.7: Longitudinal attachment welded on the surface (DNV-GL 2020, p. 142).

Table 4.2: S-N curve for class E detail in air

<i>S-N curve</i>	$N \leq 10^7$	
	m_1	$\log \bar{a}_1$
Class E	3.0	12.010

4.4.2 Cross-sectional area

As indicated in Equation 4.7, it is necessary to determine the area where the stress is distributed. It is assumed that the crack will initiate at the weld toe, and so the cross-sectional area of the specimen at this point is used. This region of the specimen is depicted in Figure 4.8, with the dimensions provided in the mechanical drawing in Appendix A.

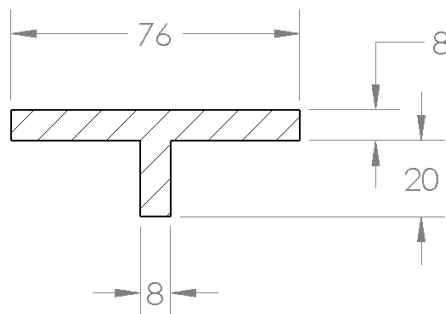


Figure 4.8: Cross section of the area under the weld toe.

4.4.3 Long-life fatigue test

For the first specimen, the plan was to perform the fatigue test using the fatigue rig with a loading capacity of 100 kN , as this was the only rig available at this moment. However, after performing the calculations, it was predicted that the specimen would probably need larger loads to reach failure in a reasonable times-span. Nevertheless, it was decided to perform one test .

The calculations were performed according to the process described in subsection 4.4.1. In this attempt, the girder was neglected from the cross-sectional area under the weld toe, resulting in $A_{red} = 608\text{ mm}^2$, and the stress ratio was reduced to $R = 0.4$ to give a larger stress range, which ended up being $\Delta S = 100.8\text{ MPa}$. It was aimed at fatigue failure after $N = 1.0 \cdot 10^6$ cycles, and the calculated load levels are included in Table 4.3. As the specimen had not reached failure after $N = 2.0 \cdot 10^6$ cycles, the fatigue test was terminated.

Table 4.3: The load levels for the first attempted fatigue test

F_m	70 kN
F_{max}	100 kN
F_{min}	40 kN

From these load levels, and from the

4.4.4 The second and final attempt

For the second test it was attempted to perform the fatigue test using a test rig with a maximum load capacity of 2000 kN . The calculations were performed according to the process described in subsection 4.4.1. It was aimed at fatigue failure after $N = 5.0 \cdot 10^4$ cycles. This resulted in the stress range $\Delta S = 273.5\text{ MPa}$. The stress ratio $R = 0.5$ was used to calculate the stress levels, because $R \geq 0.5$ is usually

applied when performing fatigue test on welded structures. The stress levels and the calculated load levels, based on the complete cross-sectional area under the weld toe $A = 768 \text{ mm}^2$, are included in Table 4.3. The result is presented in section 5.3.

Table 4.4: The load and stress levels for the final fatigue test

(a) Stress levels		(b) Load levels	
S_m	410 MPa	F_m	315 kN
S_{max}	547 MPa	F_{max}	420 kN
S_{min}	274 MPa	F_{min}	210 kN

The results are presented in section 5.3.

Chapter 5

Results

In this chapter, the resulting hot-spot stresses are limit state analyses and summarize with some concluding remarks. In addition, recommendations to further work will be given.

5.1 The hot-spot stresses

In this section the hot-spot stresses calculated from the finite element analysis and from the strain gauges are presented.

5.1.1 Hot-spot stresses for the solid model

The stresses at the hot-spot extrapolation points and the hot-spot stresses for the different load levels is presented in Table 5.1.

Table 5.1: The hot-spot stresses from the solid model

Load level [kN]	$\sigma_{0.5t}$ [MPa]	$\sigma_{1.5t}$ [MPa]	$\sigma_{hs,solid}$ [MPa]
2	5.0019	4.1789	5.4135
5	12.0362	10.4472	13.5336
10	25.0097	20.8943	27.0674

5.1.2 Hot-spot stresses from the shell model

The stresses at the hot-spot extrapolation points and the hot-spot stresses for the different load levels is presented in Table 5.2.

Table 5.2: The hot-spot stresses from the shell model

Load level [kN]	$\sigma_{0.5t}$ [MPa]	$\sigma_{1.5t}$ [MPa]	$\sigma_{hs,shell}$ [MPa]
2	4.8145	3.8831	5.2802
5	12.0362	9.7078	13.2004
10	24.0724	19.4156	26.4008

5.1.3 Hot-spot stresses from the strain gauges

The stress readings of each strain gauge is included in Appendix E. For the given load, the stresses from the strain gauges and the hot-spot stresses for the different load levels are presented.

Table 5.3: The first specimen, strain gauge 1 and 2

Load level [kN]	$\sigma_{0.5t}$ [MPa]	$\sigma_{1.5t}$ [MPa]	$\sigma_{hs,0122}$ [MPa]
2	4.2430	3.7579	4.4855
5	9.7320	8.3486	10.4237
10	18.8030	15.9180	20.2455

Table 5.4: The first specimen, strain gauge 3 and 4

Load level [kN]	$\sigma_{0.5t}$ [MPa]	$\sigma_{1.5t}$ [MPa]	$\sigma_{hs,0134}$ [MPa]
2	4.3091	3.6317	4.6478
5	9.6376	8.023	10.4449
10	18.6220	15.338	20.2640

Table 5.5: The second specimen, strain gauge 1 and 2

Load level [kN]	$\sigma_{0.5t}$ [MPa]	$\sigma_{1.5t}$ [MPa]	$\sigma_{hs,0212}$ [MPa]
2	3.957	3.193	4.3390
5	9.832	7.981	10.7575
10	19.891	15.812	21.9304

Table 5.6: The second specimen, strain gauge 3 and 4

Load level [kN]	$\sigma_{0.5t}$ [MPa]	$\sigma_{1.5t}$ [MPa]	$\sigma_{hs,0234}$ [MPa]
2	3.378	2.910	3.6120
5	8.682	7.510	9.2680
10	17.788	15.210	19.0770

5.2 Evaluate the hot-spot method

To determine whether the hot-spot method is applicable to predicting the failure, it is necessary to find out if the hot spot stress at the weld for the load range used during the fatigue test. The load range is $\Delta F = F_{max} - F_{min} = 210 \text{ kN}$. The linear-elastic material properties ensures a proportional relationship between the load range ΔF and the corresponding hot-spot stress $\Delta\sigma_{hs}$. This relationship can

be described as:

$$\Delta\sigma_{hs} = \Delta F \cdot x \quad (5.1)$$

where x is the proportionality constant. This constant x can be found for each hot-spot stress

$$x = \frac{\sigma_{hs}(F_i)}{F_i} \quad (5.2)$$

where $\sigma_{hs}(F_i)$ is the hot-spot stress resulting from the applied load F_i . The hot-spot stresses computed using Equation 5.1, along with thickness corrected value, is presented in Table 5.7.

Table 5.7: The hot-spot stress corresponding to the load range

	$\Delta\sigma_{hs,ref}$ [MPa]	$\Delta\sigma_{hs,ref}$ [MPa]
Solid	568.4	427.5
Shell	554.4	417.0
Specimen 1, SG1 and SG2	425.2	319.8
Specimen 1, SG3 and SG4	425.5	320.1
Specimen 2, SG1 and SG2	460.5	346.4
Specimen 2, SG3 and SG4	400.6	301.3

The thickness corrected values for the different hot-spot stress ranges $\Delta\sigma_{hs,ref}$ is plotted and compared with the S-N diagram for class D details in Figure 5.1 and Figure 5.2. Note that the hot-spot stresses at the brackets of the test specimen are almost identical, and therefore difficult to distinguish in Figure 5.1.

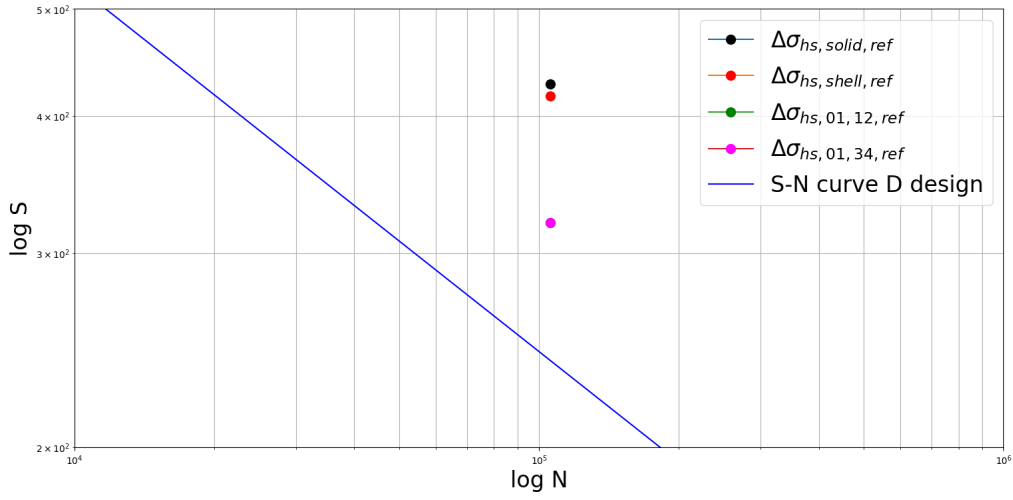


Figure 5.1: Comparison of the hot-spot method in Abaqus an specimen 1

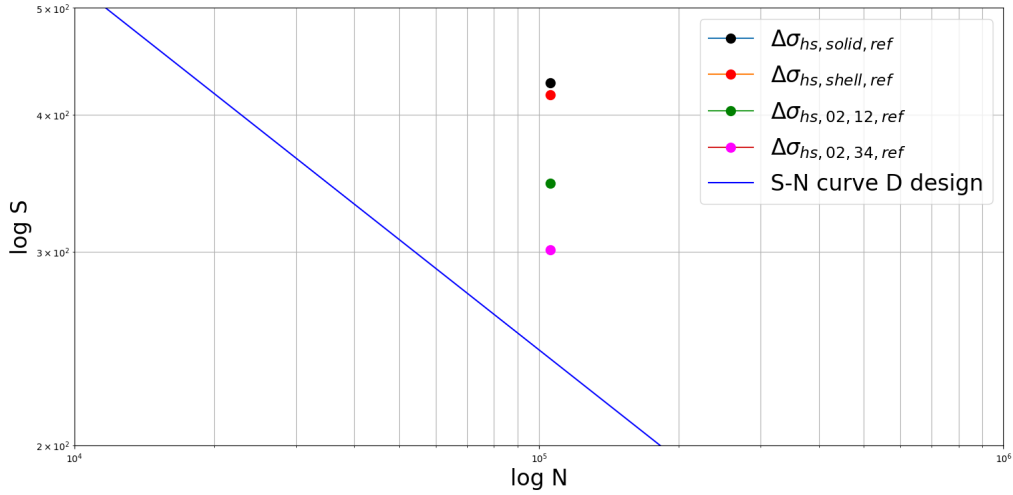


Figure 5.2: Comparison of the hot-spot method in Abaqus an specimen 2

5.3 The fatigue test

The fatigue test was performed for a stress range $\Delta S = 273.5 \text{ MPa}$, which resulted in failure after $N = 105544$ cycles. This needs to be corrected for, due to the small thickness of the plates in the specimen, using the formula for thickness effect, presented in ().

$$\Delta S_{ref} = \Delta S \left(\frac{t}{t_{ref}} \right)^k = 273.5 \text{ MPa} \cdot \left(\frac{8 \text{ mm}}{25 \text{ mm}} \right)^{0.25} = 205.7 \text{ MPa} \quad (5.3)$$

In Figure 5.3, these values are plotted and compared to the S-N diagram for class E detail:

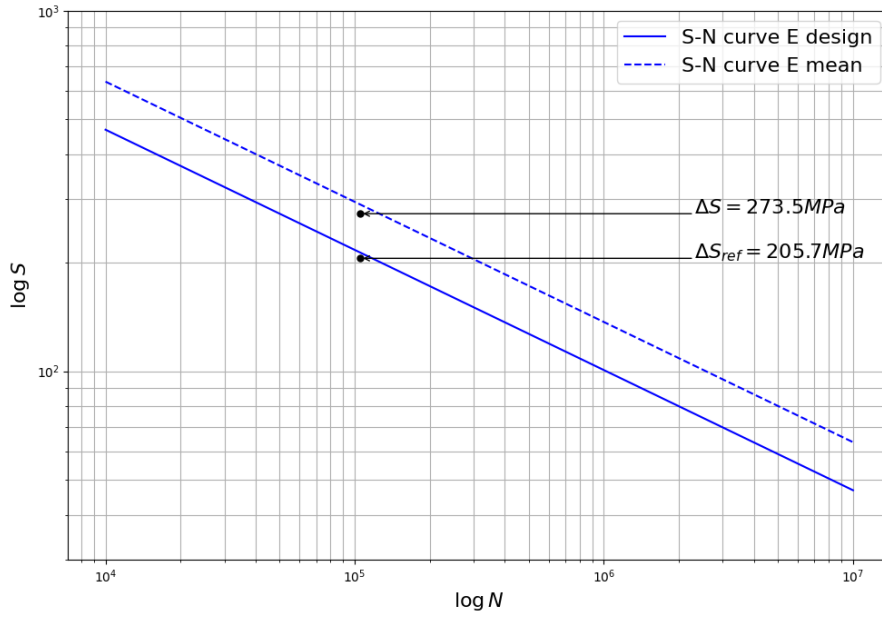


Figure 5.3: Stress range

The stress range with thickness correction ΔS_{ref} is plotted in Figure 5.4 and compared with the S-N diagram for F3:

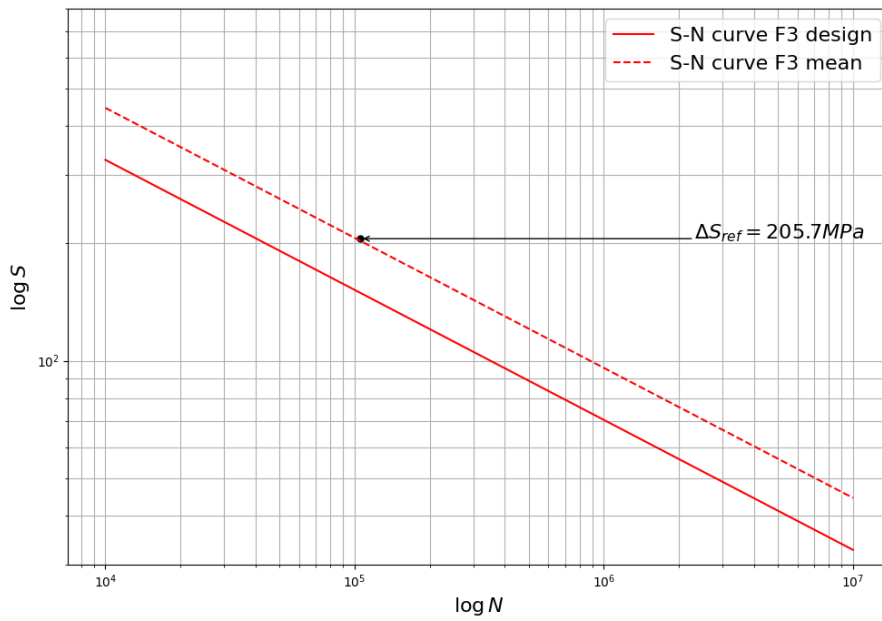


Figure 5.4: Stress range

5.3.1 Fracture surface and crack initiation

The fracture surface where the failure occurred is included in Figure 5.5.

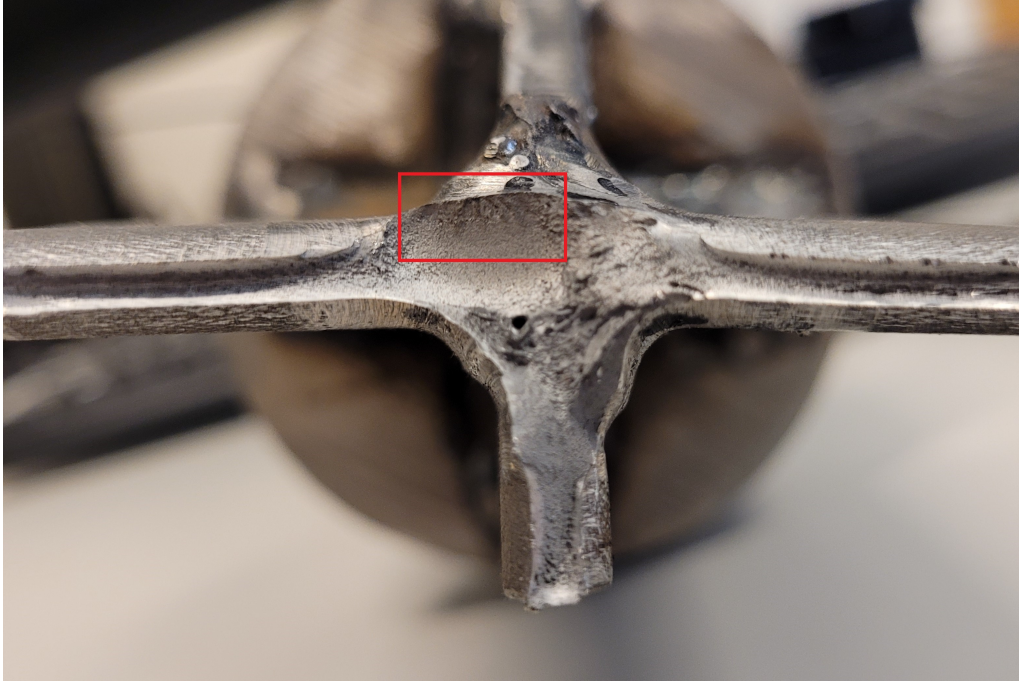


Figure 5.5: Fracture surface of specimen subjected to fatigue failure

A crack had also initiated at the opposite weld toe, as seen in Figure 5.6.



Figure 5.6: Initiation of crack on the opposite weld toe

Chapter 6

Discussion

In this chapter, the results obtained in the finite element analysis and from the experimental testings are discussed.

6.1 General remarks

Some general observations were made that solidified the basis for the results.

6.1.1 Proportional relationship between load and stress

In subsection 5.1.3 it is verified that there exists a approximately proportional relationship between the applied load and the resulting hot-spot stress at the weld toe. The relationship is considered proportional in the following calculations, because the deviation is negligible. The deviation might be a result of non-exact readings of the stress from the strain gauges, included in Appendix E.

6.1.2 Scan of specimen

As mentioned in section 4.2, the specimen were scanned in 3D using GOM Inspection software. As the scan aligns very well with the CAD model, it is assumed that the risk of bending is negligible.

It did, however, reveal that some of the dimensions of the specimen is smaller for the physical specimen compared to the CAD model. For example the lowest section of the girder has a height of 17.5 mm , as seen in the first picture included in Figure D.1, compared to 20 mm in the mechanical drawing. This leads to a smaller cross-section, which means that the load levels, calculated based on the cross-sectional area in the mechanical drawing, are larger than actually required to achieve the desired stress range. This effect is small, and is not accounted for when performing the analysis.

6.2 The hot-spot method

Comparing the S-N diagram for class D with the hot-spot stresses, all predict failure after $N = 105544$ cycles, as had occurred for the first specimen.

6.2.1 Comparing the solid and shell element

In Figure 5.1 and Figure 5.2, the hot-spot stress calculated using shell elements lies very near the value calculated using solid elements. This is very interesting, as it was considerably easier to create the model using shell elements, and additionally it reduces the computational time.

6.2.2 Comparing the different hot-spot stresses

In the S-N diagram which includes the hot-spot stresses, one can see that the finite element analysis overpredicted the values compared to the results from the strain gauges. It is desirable that the finite element analysis provides a conservative estimate of the fatigue life, but these values might be considered too high compared to the recorded values in the specimen.

One reason for lower values for the specimen, could possibly be the placement of the strain gauges farthest away from the welds. These strain gauges were supposed to be placed $1.5t = 12\text{ mm}$ from the weld toe, but were placed 16 mm from the

weld toe. When the two strain gauges are farther apart, the tangent created by linear extrapolation between the two points is less steep compared to the tangent extrapolated using the points in Abaqus.

Another reason for the deviation in the values, is that it is difficult to place the strain gauges at the correct positions, because uncertainty of the weld toe in the test specimen.

6.2.3 Comparison of the stresses in the second specimen

The hot-spot method predicts almost the same value for the hot spot stresses at the first specimen. While for the next specimen, the hot-spot stress at one of the weld toes, $\Delta\sigma_{hs,02,12,ref}$, is considerably larger than for the opposite weld toe. The different stress values recorded in the strain gauges for the second specimen are compared in Figure E.15, and here it is possible to see that there is a considerable difference between the stress reading at strain gauge 1 and strain gauge 4.

The reason for this is not clear, but could be due to uncertainty regarding the location of the weld toe. The welds are more distinguished in this specimen compared to the last, and so this could affect the stress concentration in the area. Further investigation into this could be done by subjecting this specimen to the same stress range as the first test, to find out if failure would occur at the indicated weld toe.

6.3 The fatigue test

In Equation 4.4.1 it was assumed that the bracket could be classified as a class E detail. This led to a stress range of $\Delta S = 273.5 MPa$, and failure after N cycles. According to the results of the fatigue test presented in section 5.3, the stress range corrected for the thickness effect is located under the mean curve for class E

The mean curve, as described in section 2.5, is associated with 50% survival. Therefore, based on this single fatigue test, it could indicate that the geometry produces a shorter fatigue life than what the E class predicts, making it non-conservative for his case. However, fatigue testing expected to yield scattered results. It is necessary to run more tests to be able to conclude anything.

6.3.1 High load levels

The fatigue test was performed using high load levels, which resulted in large stress levels, as seen in Table 4.4. The mean stress S_m and the maximum stress S_{max} lies significantly over the yield strength at 355 *MPa* according to (DNV-GL 2019). This means that the specimen will be hardened when stressed above this value, but the succeeding load cycles can be considered elastic, as they do not reach this newly created yield strength. There is therefore a possibility that the specimen is elongated, but this is considered negligible.

6.4 Fracture surface

When inspecting the fracture surface, as included in Figure 5.5, it is possible to recognize that the fatigue crack as the semi-circle which is highlighted in the red square. The crack most likely originated on the surface, or at least very close to the surface. It is also worth noting the decrease of cross-sectional area, which probably occurred right before the sudden fracture of the material.

Furthermore, in Figure 5.6, the crack initiated at the opposite weld toe is observed.

Chapter 7

Conclusion and further work

This chapter is meant to summarize the work with some concluding remarks. In addition, some recommendations to further work is included.

7.1 Conclusion

In this case, the hot-spot method did predict that the specimen would fail after $N = 105544$ under stress range $\Delta S = 273.5 \text{ MPa}$, even when corrected for thickness effect. The hot-spot stress calculated using shell elements lies very near the value calculated using solid elements. The fatigue test also showed that the E-curve would not be appropriate to predict calculate fatigue life for this geometry. The number of tests included in this project are not sufficient to make any firm conclusions based on the results.

7.2 Further Work

The future work of the themes discussed here could involve performing more tests as described in this thesis. More tests should be conducted to ensure a larger certainty in the test results.

This thesis considered one specific bracket geometry, and it might also be

interesting to perform similar studies on different bracket geometries. Furthermore, there are other geometries that are problematic when analysed using finite element method, and it would also be useful to gain more knowledge of accurately perform the hot-spot method on these.

There exists uncertainty regarding the effect of small thickness on fatigue life.

Bibliography

- Achintha, M. et al. (2014). «Fatigue behaviour of geometric features subjected to laser shock peening: Experiments and modelling». In: *International Journal of Fatigue* 62. 9th Fatigue Damage of Structural Materials Conference, pp. 171–179. ISSN: 0142-1123. DOI: <https://doi.org/10.1016/j.ijfatigue.2013.04.016>. URL: <https://www.sciencedirect.com/science/article/pii/S0142112313001229>.
- Antaki, George and Ramiz Gilada (2015). «Chapter 2 - Design Basis Loads and Qualification». In: *Nuclear Power Plant Safety and Mechanical Integrity*. Ed. by George Antaki and Ramiz Gilada. Boston: Butterworth-Heinemann, pp. 27–102. ISBN: 978-0-12-417248-7. DOI: <https://doi.org/10.1016/B978-0-12-417248-7.00002-3>. URL: <https://www.sciencedirect.com/science/article/pii/B9780124172487000023>.
- Berge, Stig (1985). «On the effect of plate thickness in fatigue of welds». In: *Engineering Fracture Mechanics* 21.2, pp. 423–435. ISSN: 0013-7944. DOI: [https://doi.org/10.1016/0013-7944\(85\)90030-X](https://doi.org/10.1016/0013-7944(85)90030-X). URL: <https://www.sciencedirect.com/science/article/pii/001379448590030X>.
- Berge, Stig and Sigmund Kyrre Ås (2017). *Compendium - Fatigue and Fracture Design of Marine Structures*. eng. 3rd ed. NTNU - Faculty of Engineering Science and Technology.
- Dassault Systèmes (2008). *ABAQUS/Standard User's Manual, Version 6.8*. English. United States: Dassault Systèmes Simulia Corp.
- DNV-GL (July 2019). *Metallic materials DNVGL-OS-B101*. Technical Report. Det Norske Veritas.

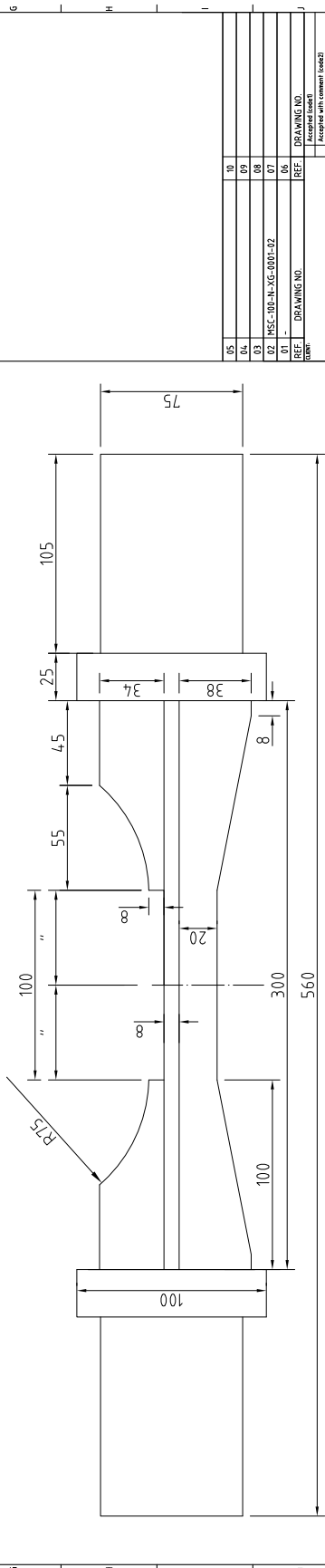
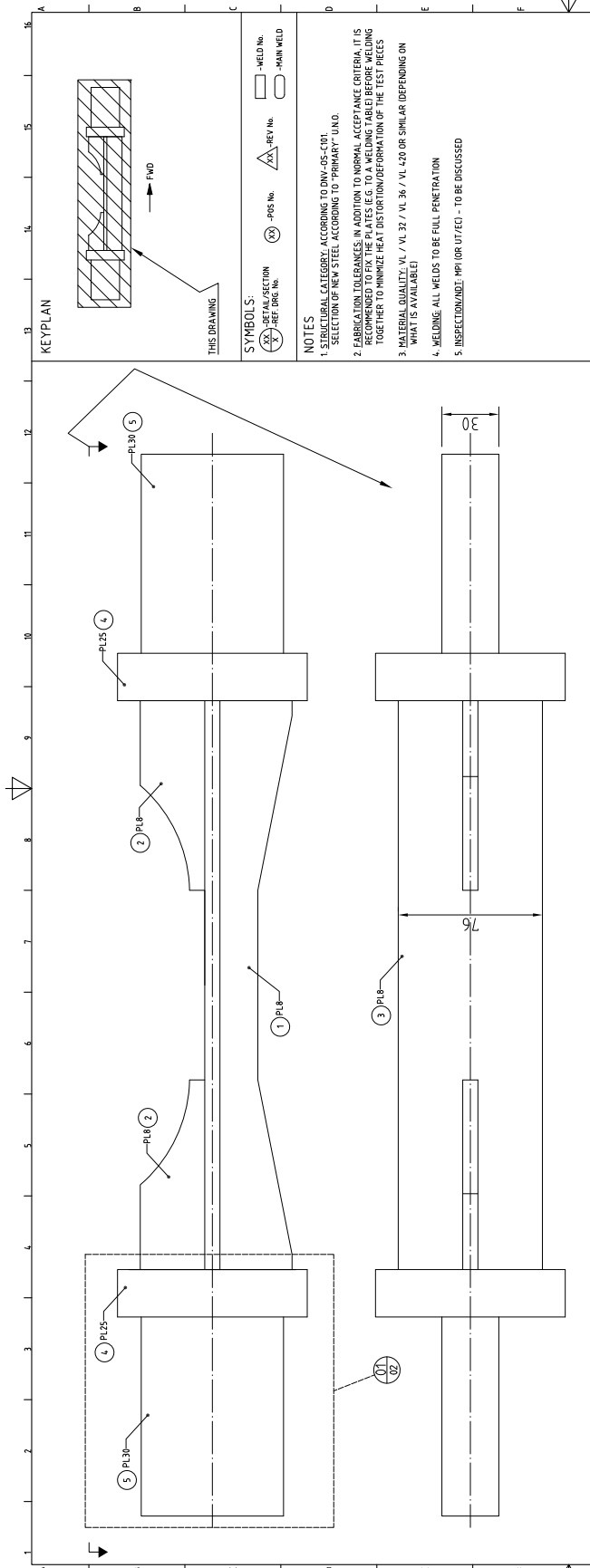
- DNV-GL (Apr. 2020). *Fatigue Design of Offshore Steel Structures, Recommended Practice DNVGL-RP-C203*. Technical Report. Det Norske Veritas.
- Dowling, Norman E. (2013). *Mechanical behavior of materials : engineering methods for deformation, fracture, and fatigue*. eng. 4th ed., international ed. contributions by Katakam Siva Prasad, R. Narayanasamy. Boston, Mass: Pearson Education. ISBN: 9780131395060.
- Fricke, Wolfgang (July 2008). *Guideline for the Fatigue Assessment by Notch Stress Analysis for Welded Structures*.
- Hobbacher, A. F (2016). *Recommendations for Fatigue Design of Welded Joints and Components*. eng. IIW Collection. Cham: Springer International Publishing AG. ISBN: 9783319237565.
- Irving, S. et al. (2005). «Comparative fatigue assessment of soft toe and nested bracket welded aluminium structures». In: *Engineering Failure Analysis* 12.5. ICEFAI Part I, pp. 679–690. ISSN: 1350-6307. DOI: <https://doi.org/10.1016/j.engfailanal.2004.12.005>. URL: <https://www.sciencedirect.com/science/article/pii/S1350630705000257>.
- Lee, Jae-Myung et al. (2010). «Comparison of hot spot stress evaluation methods for welded structures». In: *International Journal of Naval Architecture and Ocean Engineering* 2.4, pp. 200–210. ISSN: 2092-6782. DOI: <https://doi.org/10.2478/IJNAOE-2013-0037>. URL: <https://www.sciencedirect.com/science/article/pii/S2092678216302497>.
- Leonard P. Connor R. L. O'Brien, American Welding Society (1991). *Welding Handbook: WELDING PROCESS VOLUME 2 8th edition*. 8th ed. American Welding Society. ISBN: 9780871713544.
- Lotsberg, Inge (2016). *Fatigue design of marine structures*. eng. New York NY: Cambridge University Press. ISBN: 9781107121331.
- Mecseri, Balázs and B. Kövesdi (Apr. 2020). «Discussion on the Hot-Spot and Notch Stress Based Fatigue Assessment Methods Based on Test Results». In: *International Journal of Steel Structures* 20. DOI: 10.1007/s13296-020-00345-1.

- Mikkola, Eeva, Yukitaka Murakami, and Gary Marquis (2014). «Fatigue Life Assessment of Welded Joints by the Equivalent Crack Length Method». In: *Procedia Materials Science* 3. 20th European Conference on Fracture, pp. 1822–1827. ISSN: 2211-8128. DOI: <https://doi.org/10.1016/j.mspro.2014.06.294>. URL: <https://www.sciencedirect.com/science/article/pii/S2211812814002958>.
- Niemi, E. (1995). *Stress determination for fatigue analysis of welded components*. eng. Abington.
- Niemi, Erkki, Wolfgang Fricke, and Stephen Maddox (2018). *Structural Hot-Spot Stress Approach to Fatigue Analysis of Welded Components: Designer's Guide*. Springer. ISBN: 978-981-10-5567-6.
- Radaj, D., C.M. Sonsino, and W. Fricke (2009). «Recent developments in local concepts of fatigue assessment of welded joints». In: *International Journal of Fatigue* 31.1. Fatigue assessment of welded connections, pp. 2–11. ISSN: 0142-1123. DOI: <https://doi.org/10.1016/j.ijfatigue.2008.05.019>. URL: <https://www.sciencedirect.com/science/article/pii/S0142112308001540>.
- Radaj, Dieter (1990). *Design and analysis of fatigue resistant welded structures*. eng. Cambridge: Abington Publ. ISBN: 1855730049.
- Ringsberg, Jonas et al. (June 2014). «Fatigue Failure Analysis of Fillet Welded Joints Used in Offshore Structures». In: *Proceedings of the International Conference on Offshore Mechanics and Arctic Engineering - OMAE* 4. DOI: 10.1115/OMAE2014-23166.
- Sonsino, C.M. et al. (2012). «Notch stress concepts for the fatigue assessment of welded joints – Background and applications». In: *International Journal of Fatigue* 34.1. Modern Local Design Concepts for the Fatigue Assessment of Welded Structures – Industrial Applications, pp. 2–16. ISSN: 0142-1123. DOI: <https://doi.org/10.1016/j.ijfatigue.2010.04.011>. URL: <https://www.sciencedirect.com/science/article/pii/S0142112310001131>.

Suresh, S. (1998). *Fatigue of Materials*. 2nd ed. Cambridge University Press. ISBN:
9780511806575.

Appendix A

Technical drawing of bracket toe



SYMBOLS:

REF. SECTION	POS. No.	REV. No.	WELD No.
REF. DRG. No.			MAIN WELD

NOTES:

- STRUCTURAL CATEGORY: ACCORDING TO DNV-OS-C101.
- SELECTION OF NEW STEEL ACCORDING TO "PRIMARY" U.L.N.O.
- FABRICATION TOLERANCES IN ADDITION TO NORMAL ACCEPTANCE CRITERIA. IT IS RECOMMENDED TO TAKE INTO ACCOUNT THE WELDING TOGETHER TO MINIMIZE HEAT DISTORTION/DEFORMATION OF THE TEST PIECES.
- MATERIAL QUALITY: VL / VL 32 / VL 36 / VL 420 OR SIMILAR (DEPENDENT ON WHAT IS AVAILABLE)
- WELDING ALL WELDS TO BE FULL PENETRATION
- INSPECTION/NDT: MPI (OR UT/FT) - TO BE DISCUSSED

KEYPLAN

THIS DRAWING

PROJ. MASTER 2022 - BRACKET TOE

REV	DATE	DESCRIPTION	CREATED	CHECKED	APPROVED
02	05.10.2021	RE-ISSUED FOR CONSTR.	AF	RHR	AF
01	04.10.2021	ISSUED FOR CONSTRUCTION	AF	RHR	AF

NO.	PLS. DIMENSION	MAT. R.	IND. (DIP)	TOT. WEIGHT (kg)
1	PL.8			
2	PL.8			
3	PL.25			
4	PL.25			
5	PL.30			

PROJECT	MASTER 2022 - BRACKET TOE	DATE	
PROJECT DRAW. No.		SCALE	1:1
DESIGNER		U.N.O.	
CHECKED		DATE	
APPROVED			

GENERAL TOLERANCES UNLESS SPECIFIED:

Dimension	Tolerance
0 - 10	±0.1
10 - 30	±0.15
30 - 100	±0.2
100 - 300	±0.3
300 - 1000	±0.4

FABRICATION TOLERANCES: DNV-OS-C447

INSPECTION/NDT: MPI (OR UT/FT) - TO BE DISCUSSED

WELDING ALL WELDS TO BE FULL PENETRATION

REVISIONS:

NO.	DATE	DESCRIPTION	CREATED	CHECKED	APPROVED
02	05.10.2021	RE-ISSUED FOR CONSTR.	AF	RHR	AF
01	04.10.2021	ISSUED FOR CONSTRUCTION	AF	RHR	AF

KEYPLAN

THIS DRAWING

PROJ. MASTER 2022 - BRACKET TOE

REV. DATE DESCRIPTION CREATED CHECKED APPROVED

NO. DIMENSION MAT. R. IND. (DIP) TOT. WEIGHT (kg)

PLS. DIMENSION MAT. R. IND. (DIP) TOT. WEIGHT (kg)

1 PL.8 2 PL.8 3 PL.25 4 PL.25 5 PL.30

REVISIONS:

NO.	DATE	DESCRIPTION	CREATED	CHECKED	APPROVED
02	05.10.2021	RE-ISSUED FOR CONSTR.	AF	RHR	AF
01	04.10.2021	ISSUED FOR CONSTRUCTION	AF	RHR	AF

GENERAL TOLERANCES UNLESS SPECIFIED:

Dimension	Tolerance
0 - 10	±0.1
10 - 30	±0.15
30 - 100	±0.2
100 - 300	±0.3
300 - 1000	±0.4

FABRICATION TOLERANCES: DNV-OS-C447

INSPECTION/NDT: MPI (OR UT/FT) - TO BE DISCUSSED

WELDING ALL WELDS TO BE FULL PENETRATION

REVISIONS:

NO.	DATE	DESCRIPTION	CREATED	CHECKED	APPROVED
02	05.10.2021	RE-ISSUED FOR CONSTR.	AF	RHR	AF
01	04.10.2021	ISSUED FOR CONSTRUCTION	AF	RHR	AF

KEYPLAN

THIS DRAWING

PROJ. MASTER 2022 - BRACKET TOE

REV. DATE DESCRIPTION CREATED CHECKED APPROVED

NO. DIMENSION MAT. R. IND. (DIP) TOT. WEIGHT (kg)

PLS. DIMENSION MAT. R. IND. (DIP) TOT. WEIGHT (kg)

1 PL.8 2 PL.8 3 PL.25 4 PL.25 5 PL.30

REVISIONS:

NO.	DATE	DESCRIPTION	CREATED	CHECKED	APPROVED
02	05.10.2021	RE-ISSUED FOR CONSTR.	AF	RHR	AF
01	04.10.2021	ISSUED FOR CONSTRUCTION	AF	RHR	AF

GENERAL TOLERANCES UNLESS SPECIFIED:

Dimension	Tolerance
0 - 10	±0.1
10 - 30	±0.15
30 - 100	±0.2
100 - 300	±0.3
300 - 1000	±0.4

FABRICATION TOLERANCES: DNV-OS-C447

INSPECTION/NDT: MPI (OR UT/FT) - TO BE DISCUSSED

WELDING ALL WELDS TO BE FULL PENETRATION

REVISIONS:

NO.	DATE	DESCRIPTION	CREATED	CHECKED	APPROVED
02	05.10.2021	RE-ISSUED FOR CONSTR.	AF	RHR	AF
01	04.10.2021	ISSUED FOR CONSTRUCTION	AF	RHR	AF

KEYPLAN

THIS DRAWING

PROJ. MASTER 2022 - BRACKET TOE

REV. DATE DESCRIPTION CREATED CHECKED APPROVED

NO. DIMENSION MAT. R. IND. (DIP) TOT. WEIGHT (kg)

PLS. DIMENSION MAT. R. IND. (DIP) TOT. WEIGHT (kg)

1 PL.8 2 PL.8 3 PL.25 4 PL.25 5 PL.30

REVISIONS:

NO.	DATE	DESCRIPTION	CREATED	CHECKED	APPROVED
02	05.10.2021	RE-ISSUED FOR CONSTR.	AF	RHR	AF
01	04.10.2021	ISSUED FOR CONSTRUCTION	AF	RHR	AF

GENERAL TOLERANCES UNLESS SPECIFIED:

Dimension	Tolerance
0 - 10	±0.1
10 - 30	±0.15
30 - 100	±0.2
100 - 300	±0.3
300 - 1000	±0.4

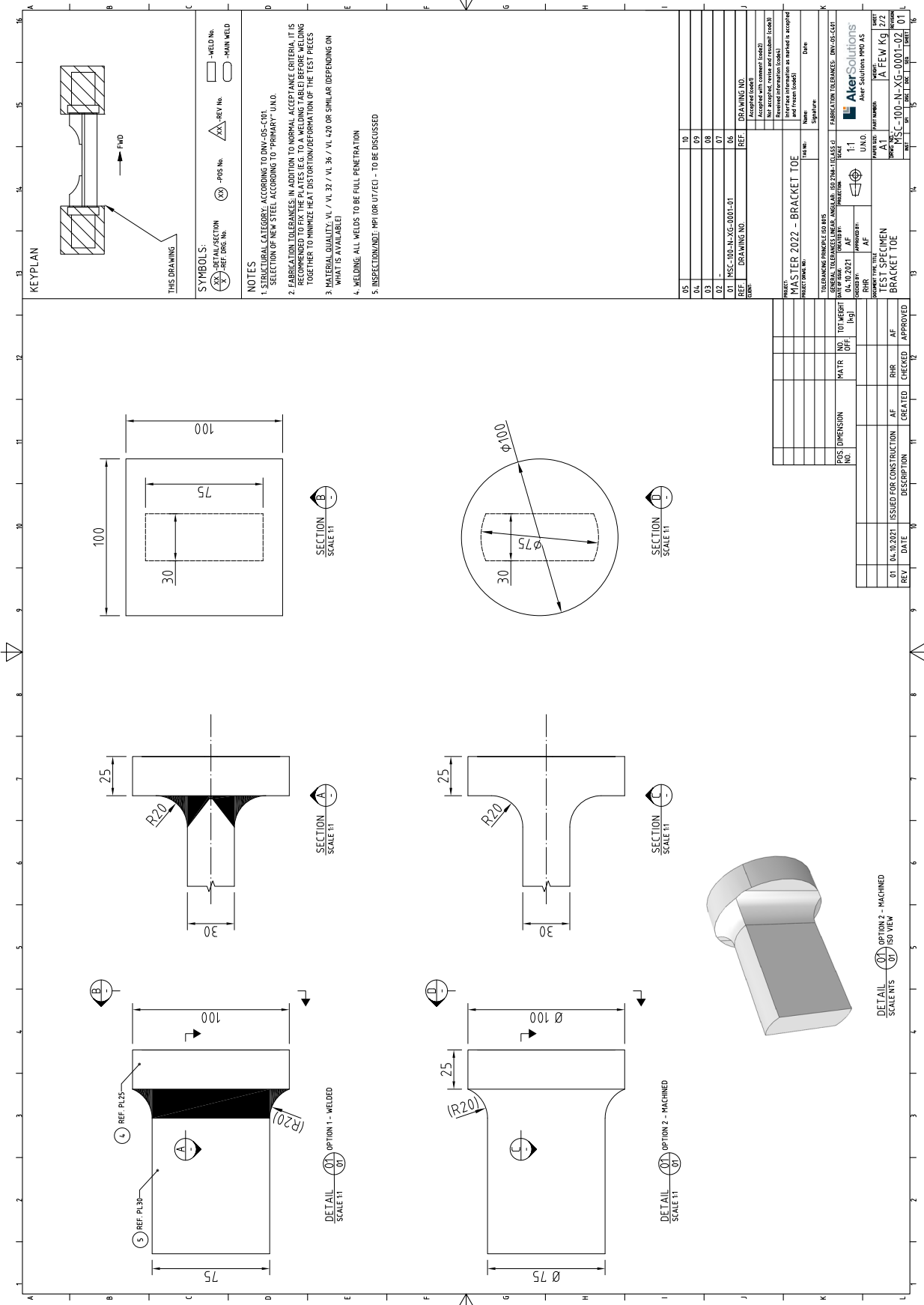
FABRICATION TOLERANCES: DNV-OS-C447

INSPECTION/NDT: MPI (OR UT/FT) - TO BE DISCUSSED

WELDING ALL WELDS TO BE FULL PENETRATION

REVISIONS:

NO.	DATE	DESCRIPTION	CREATED	CHECKED	APPROVED
02	05.10.2021	RE-ISSUED FOR CONSTR.	AF	RHR	AF
01	04.10.2021	ISSUED FOR CONSTRUCTION	AF	RHR	AF



05	10
06	09
07	08
08	07
09	06
10	05

PROJECT: MASTER 2022 - BRACKET TOE
 PROJECT NO.:
 TITLE No.:
 Name:
 Date:
 Signature:

TOLERANCE PRINCIPLE: AS AFE
 GENERAL TOLERANCES: LINEAR: ANGULAR: ISO 2768-1 CLASS: J
 DATE OF ISSUE: 04.10.2021
 DRAWING NO.:
 REV. NO.:
 DRAWING NO.:
 REV. NO.:

FABRICATION TOLERANCES: DNV-OS-C101

SCALE: 1:1

U.N.O.:

PROJECT NO.: MSC-100-N-XG-0001-02

REV. NO.:

DATE:

DESCRIPTION:

ISSUED FOR CONSTRUCTION

CREATED

CHECKED

APPROVED

Appendix B

Weld geometry

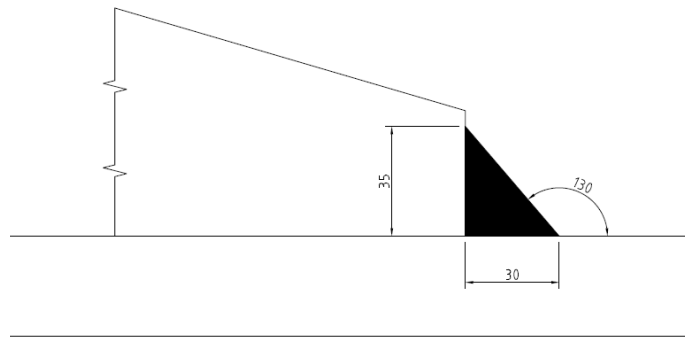


Figure B.1: Weld geometry for a 50 mm thick plate, provided by Aker Solutions

B.1 Calculating the new weld geometry

The ratio between a 8 mm thick plate and a 50 mm:

$$\frac{8 \text{ mm}}{50 \text{ mm}} = 0.16 \quad (\text{B.1})$$

The the vertical weld leg length:


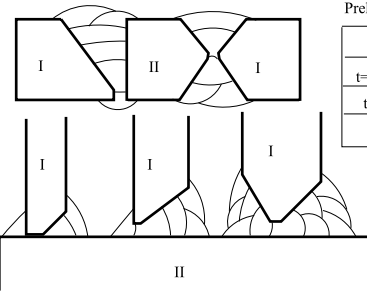
$$35 \text{ mm} \cdot 0.16 = 5.6 \text{ mm} \quad (\text{B.2})$$

The horizontal weld leg length:

$$30 \text{ mm} \cdot 0.16 = 4.8 \text{ mm} \quad (\text{B.3})$$

Appendix C

Welding procedure specification

		WELDING PROCEDURE SPECIFICATION (WPS) <i>Sveiseprosedyrespesifikasjon (WPS)</i>				WPS no.: 80-02 Ref.: Date: 11.12.19 Rev: 8																	
Prod. by: Kværner AS Project: BASIS Location: Stord sites		Client: Ref. spec.: NORSOK M-101 Ref. WPQR: 80-001 80-002 80-02 80-03		Ref. stand: EN ISO 15609-1 Exam. body:																			
Welding process Sveisemetode Shielding gas type Beskyttelsesgass type Weaving (yes/no) Pending (ja/nei)		136 M21 (Ar+18-22%CO2) Yes max.: 20 mm		2 max.: mm		3 max.: mm																	
Purging gas type Røttings type Welding positions Sveisestillinger Joint type Forbindelsestype Joint preparation Fugelåddning Cleaning method Rengjøringsmetode Backing Mothold Single/Double En-/Tosidig Back gouging Oppflating Flux designation Pulverbetegnelse Flux handling Pulverbehandling Tungsten electrode Wolframelektrode Torch angle Pistolvinkel Stand off distance Dyseavstand Nozzle diameter(s) Dyse diameter		n/a PA, PB PC, PD PE, PF H-L045 BW, T-BW, FW Grinding / Sliping Wire brush / stålborste n/a bs Arc air / kolstift n/a n/a n/a n/a n/a ° 15-20 mm 14-19 mm		EXAMPLES / EKSEMPLER:  Preheating / Forvarming <table border="1"> <tr><td>t = 3-20 mm</td><td>5 °C</td></tr> <tr><td>t = 21 - 50 mm</td><td>30 °C</td></tr> <tr><td>t > 50 mm</td><td>51 °C</td></tr> <tr><td>Rep.</td><td>+ 50 °C</td></tr> </table> Gas nozzle/ Gasshylse: 1 / min: <table border="1"> <tr><td>19 mm</td><td>18-25</td></tr> <tr><td>16 mm</td><td>14-20</td></tr> <tr><td>14 mm</td><td>12-17</td></tr> </table>				t = 3-20 mm	5 °C	t = 21 - 50 mm	30 °C	t > 50 mm	51 °C	Rep.	+ 50 °C	19 mm	18-25	16 mm	14-20	14 mm	12-17		
t = 3-20 mm	5 °C																						
t = 21 - 50 mm	30 °C																						
t > 50 mm	51 °C																						
Rep.	+ 50 °C																						
19 mm	18-25																						
16 mm	14-20																						
14 mm	12-17																						
Identification of parent metal Identifikasjon av grunnmateriale		I: CE max.: 0,47 C max.: 0,20 II: CE max.: 0,47 C max.: 0,20		PCM max.: PCM maks.:																			
Part Del		Name/grade Betegnelse		Standard Standard		Group Gruppe		Delivery condition Leveringsstilling		Thickness range Tykkelsesområde [mm]		Diameter range Diameterområde [mm]											
I		420 / lower grades		420 / lavere grader		2.1				3,00 - 100,0		40,00 - 99999											
II		420 / lower grades		420 / lavere grader		2.1				3,00 - 100,0		40,00 - 99999											
Identification of filler metal Identifikasjon av tilsett		Index Indeks		Trade name Handelsnavn		Classification Standard/klassifisering		Group Gruppe		Filler handling Tilsetthåndtering													
1		NSSW SF-3AM		AWS A5.36 E81T9-M21A8-Ni1-H4		FM1		02-W-COZ012E															
2																							
3																							
Welding parameters Sveiseparametere		Equipment: n/a Utstyr																					
Pass no. Streng nr.		Index Indeks		Dia. Dia. [mm]		Welding process Sveiseprosess		Wire feed speed Tråd- hastighet [m/min]		Current Strøm [A]		Voltage Spenning [V]		Current polarity Polaritet		Welding speed Sveisehastighet [mm/min]		Run-out length Strekk- lengde [mm]		Gas Gass [l/min]		Heat input Varmetilførsel [kJ/mm]	
1-n		1		1,20		136		6,00 - 8,00		180 - 240		21,0 - 24,0		DC+		130 - 275				1,0 - 2,3			
1-n		1		1,20		136		7,00 - 11,0		220 - 290		22,0 - 25,0		DC+		280 - 550				0,7 - 1,5			
1-n		1		1,00		136		6,00 - 11,0		130 - 220		19,0 - 23,0		DC+		120 - 320				0,7 - 2,3			
t<7:																							
1-n		1		1,20		136		5,00 - 7,00		160 - 210		19,0 - 23,0		DC+		120 - 225				0,9 - 2,2			
1-n		1		1,20		136		6,50 - 9,50		190 - 250		20,0 - 24,0		DC+		250 - 550				0,6 - 1,3			
1-n		1		1,00		136		6,00 - 10,0		130 - 200		19,0 - 22,0		DC+		120 - 320				0,5 - 2,0			
Heat treatment Varmebehandling		Method: Heat.torch/ Varmebend Metode:																					
Preheat min.: Forvarme min.:		5 °C		Interpass temp. max.: Mellonstr. temp. maks.:		250 °C		Heat treatment proc.: Varmebehandling pros.:		n/a		Temp. control: Temp. kontroll:		Temperature crayon									
PWHT min.: PWHT min.:		°C max.:		°C		Soaking: Holdetid:		min/mm		min.:		min		Heating rate: Oppv. hast.:		°C/t		Cooling rate: Avkj. hast.:		°C/t			
Remarks: Merknader:		Additional information enclosed (Yes/No): No Tilleggsinformasjon vedlagt (Ja/Nei):																					
Group / gruppe: Also / også 1. Heat treatment Method: Electric for thicknesses above 50 mm. Additional Information in Prod. Handbook, 02-W-COZ012E.		Date/signature 11.12.19 Dato/signatur: Terje O. Bruket Approved 11.12.19 Godkjent: Terje O. Bruket																					
Ref. WPQR: Also 80-042, 80-043, 80-044, 80-049, CTOD WPQR no. VSI60C02-60 and VSI60F02-100B.																							

Appendix D

3D scan of specimen 1 using GOM Inspect

The colours and plotted labels indicate misalignment compared to the solid model.

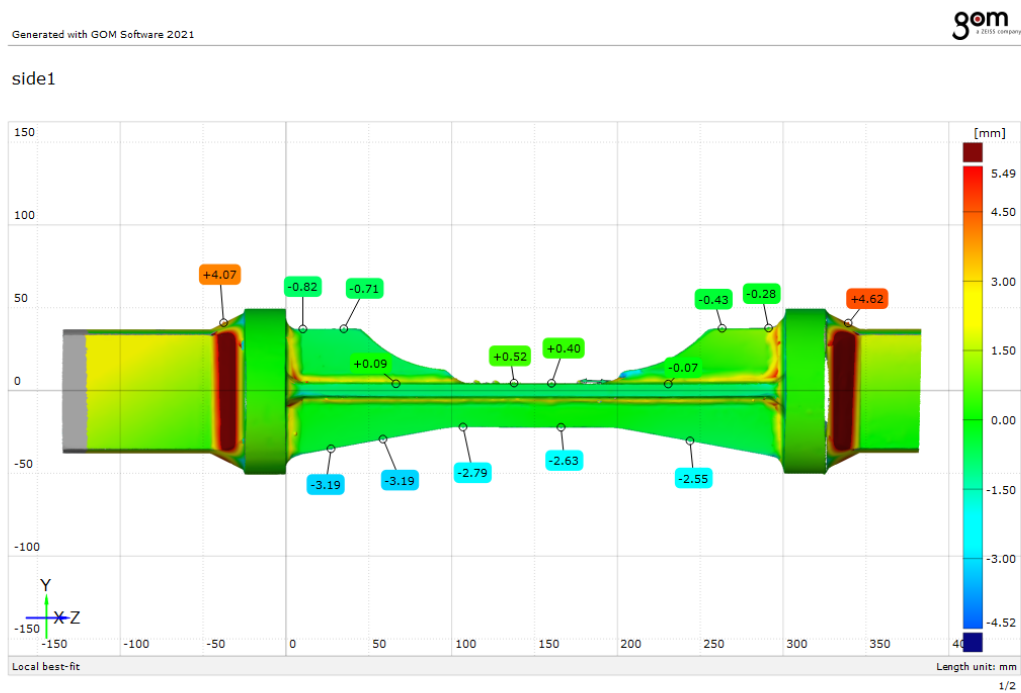


Figure D.1: 3D scan - from the side

side2

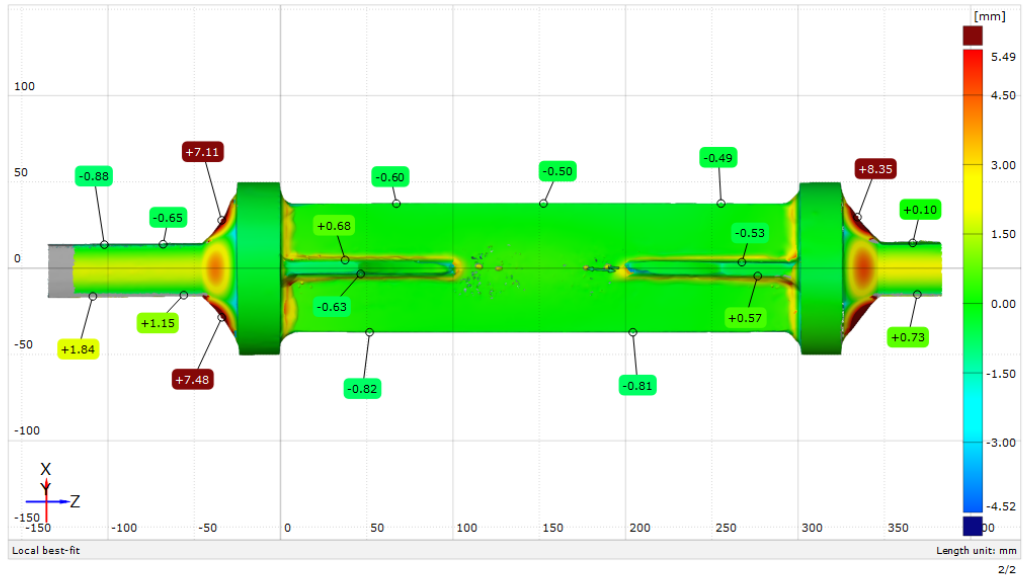


Figure D.2: 3D scan - from the top

Appendix E

Stress levels recorded in the strain gauges

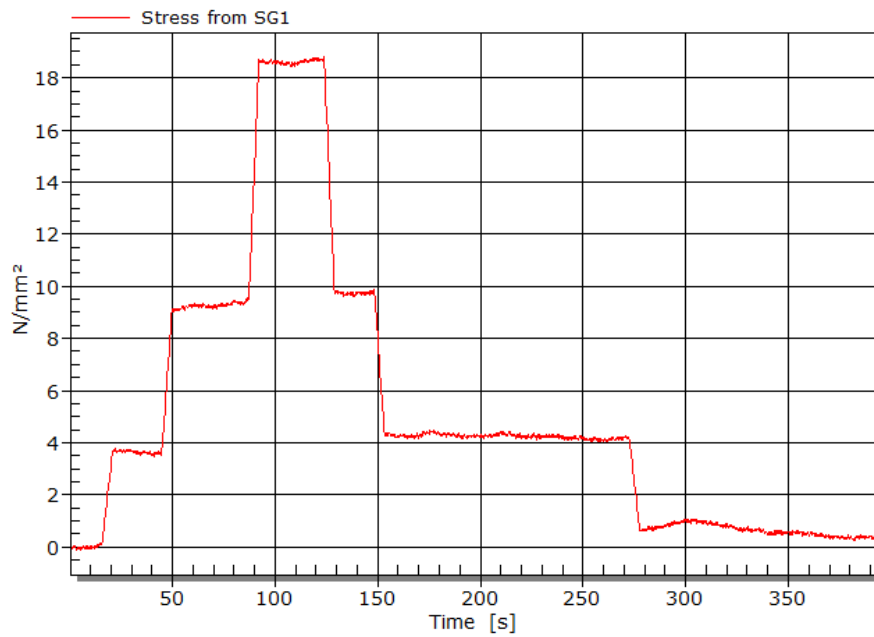


Figure E.1: Specimen 1 - Stress in strain gauge 1

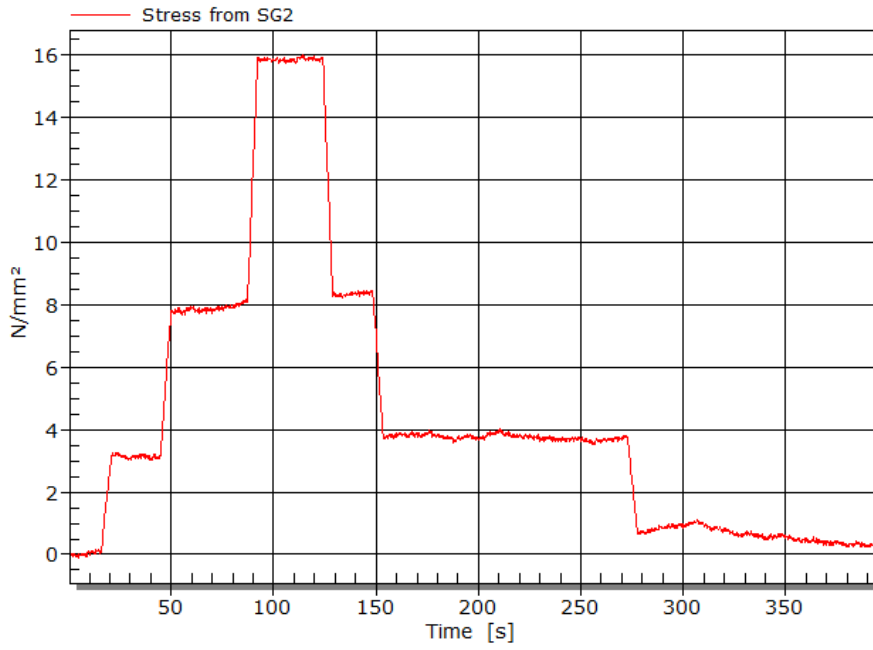


Figure E.2: Specimen 1 - Stress in strain gauge 2

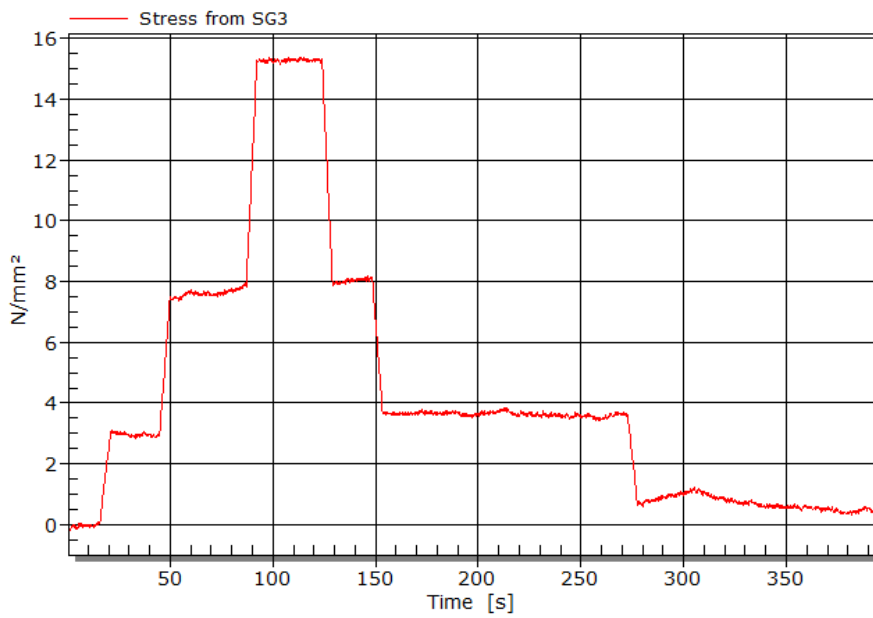


Figure E.3: Specimen 1 - Stress in strain gauge 3

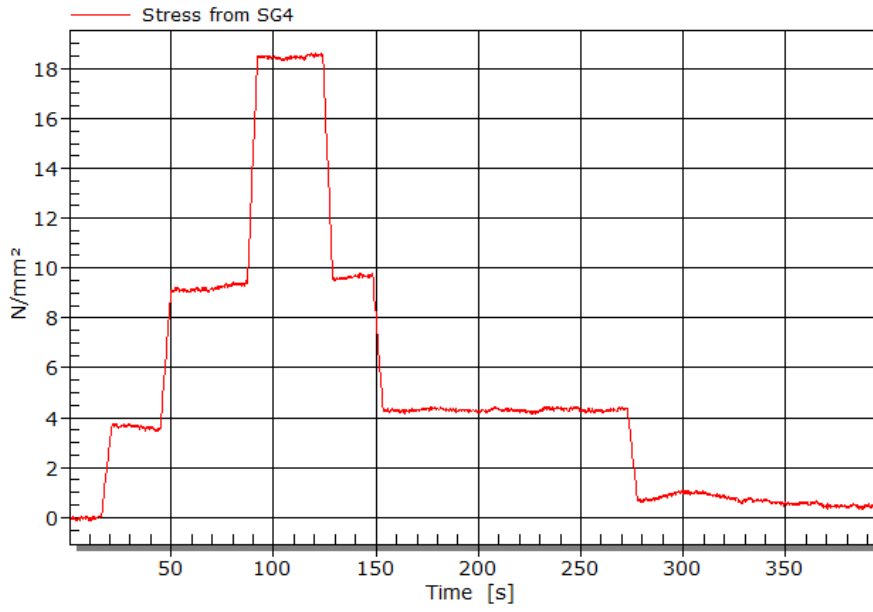


Figure E.4: Specimen 1- Stress in strain gauge 4

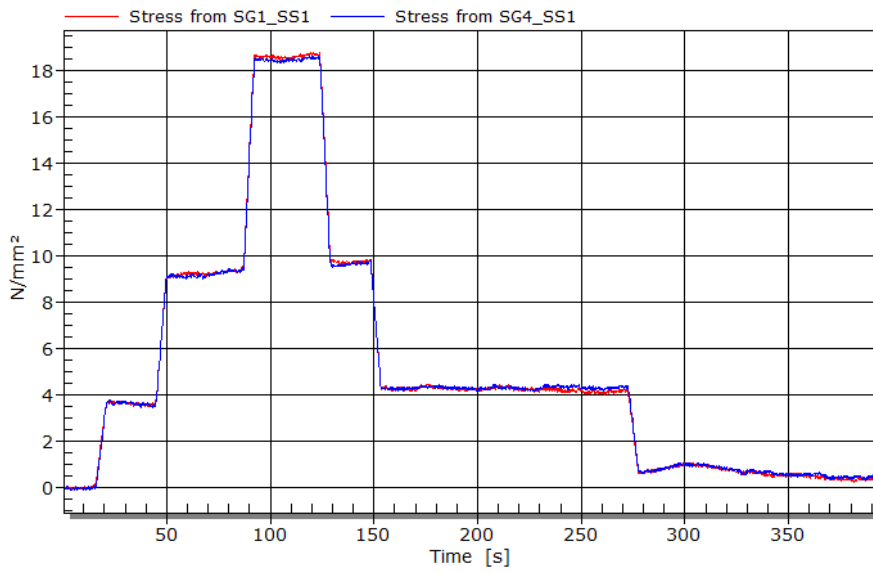


Figure E.5: Specimen 1 - Stress in strain gauge 1 and 4

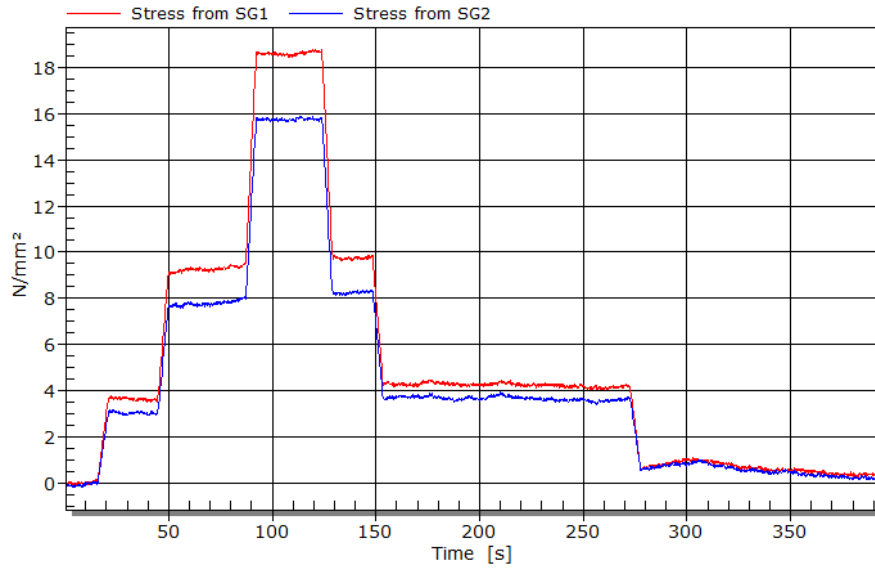


Figure E.6: Specimen 1 - Stress in strain gauge 1 and 2

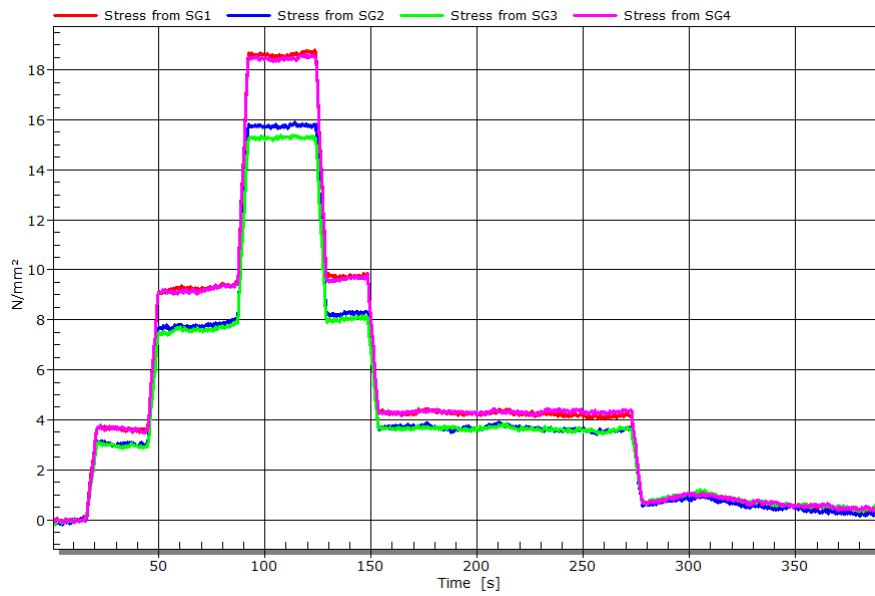


Figure E.7: Specimen 1 - Stress in strain gauge 1, 2, 3 and 4

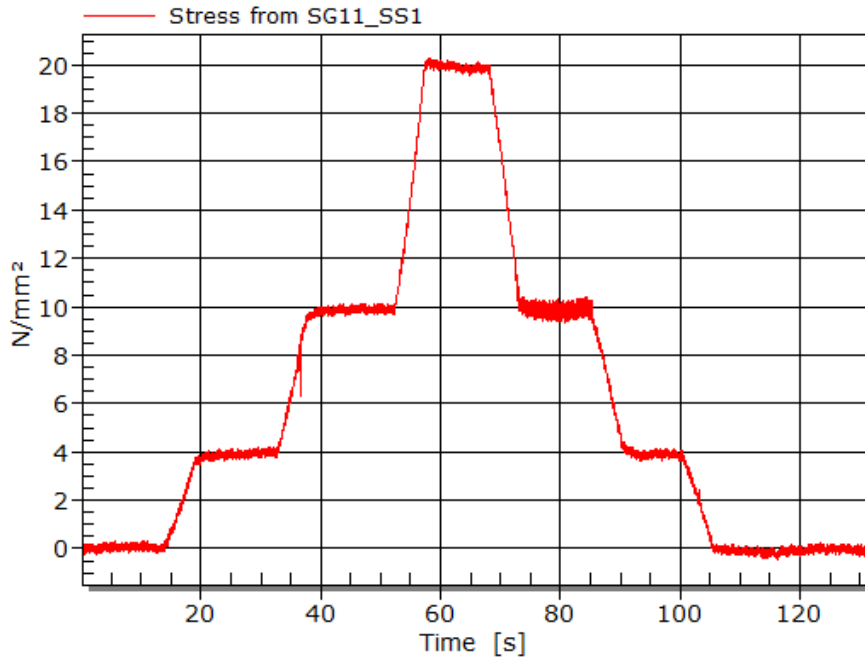


Figure E.8: Specimen 2 - Stress in strain gauge 1

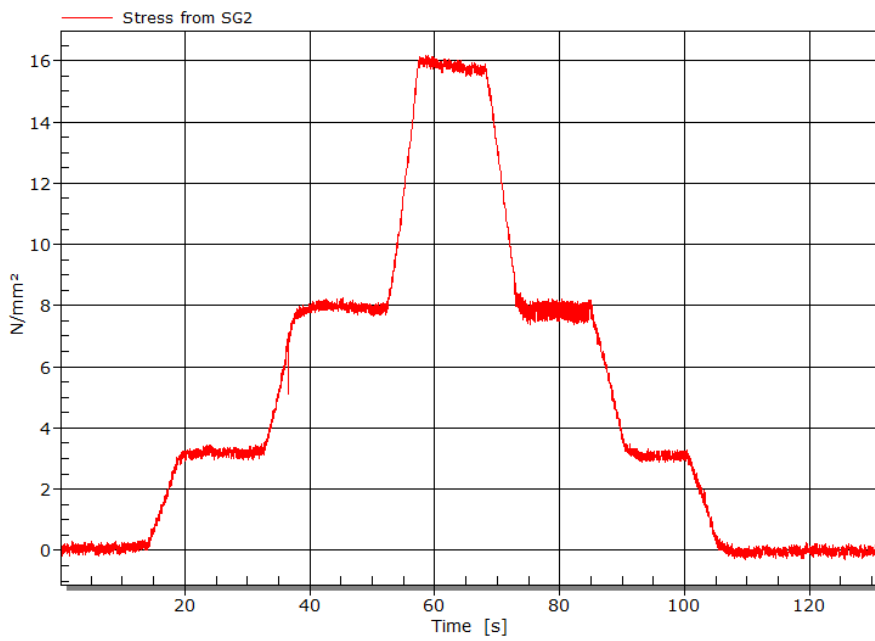


Figure E.9: Specimen 2 - Stress in strain gauge 2

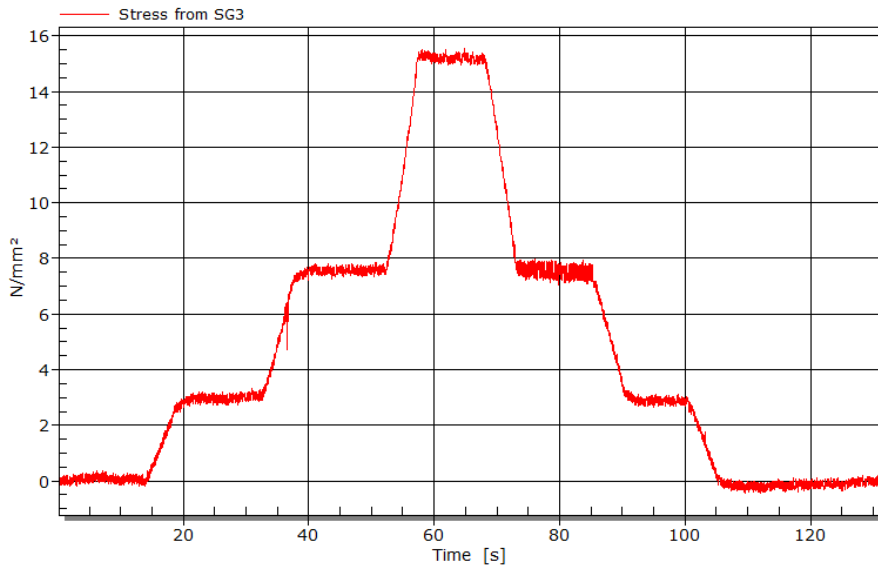


Figure E.10: Specimen 2 - Stress in strain gauge 3

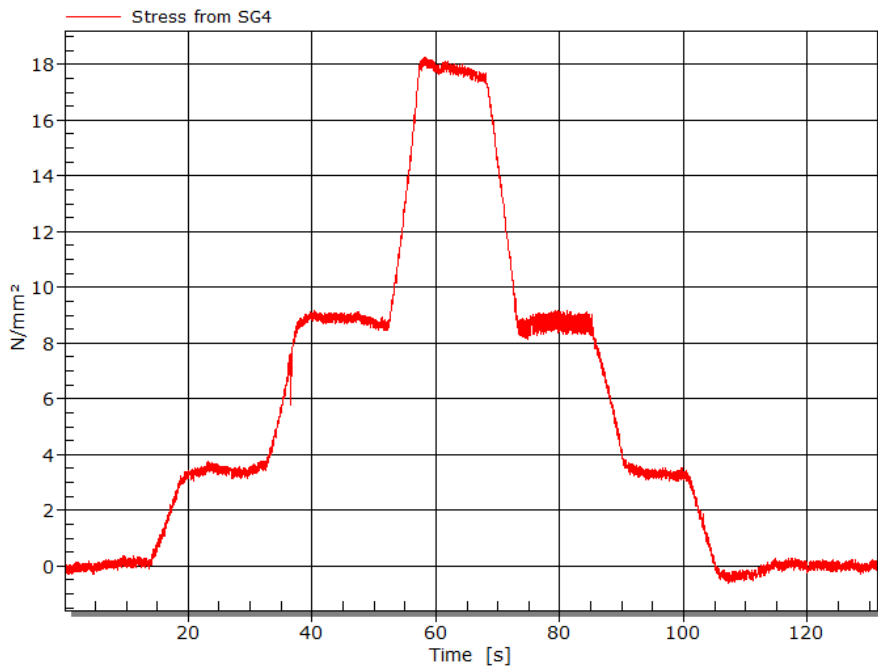


Figure E.11: Specimen 2 - Stress in strain gauge 4

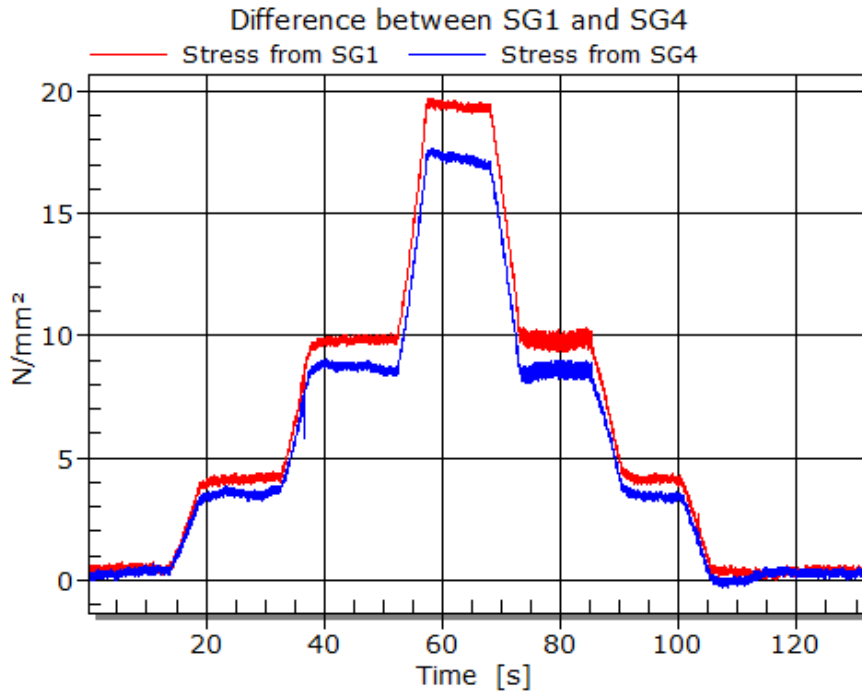


Figure E.12: Specimen 2 - Stress in strain gauge 1 and 4

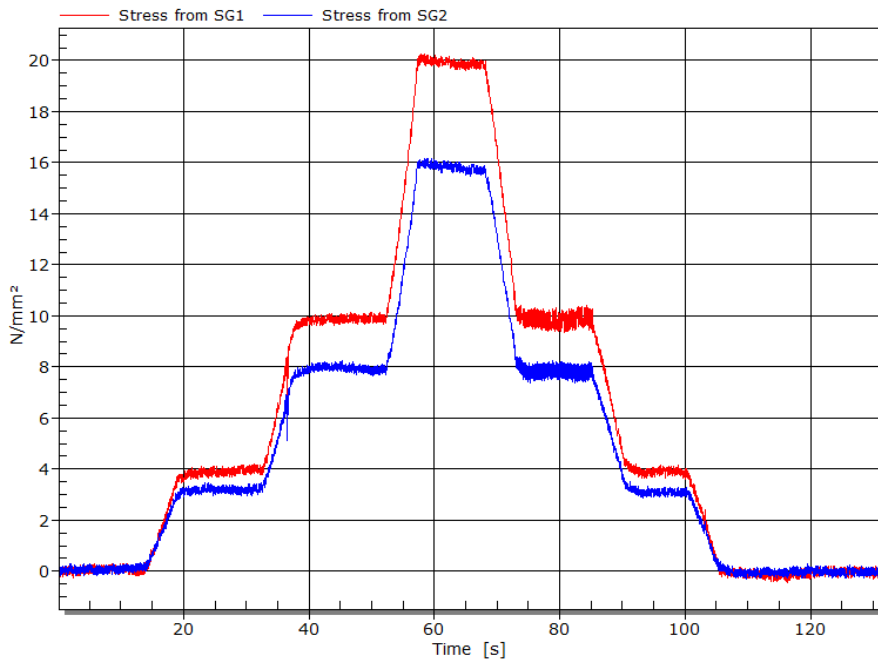


Figure E.13: Specimen 2 - Stress in strain gauge 1 and 2

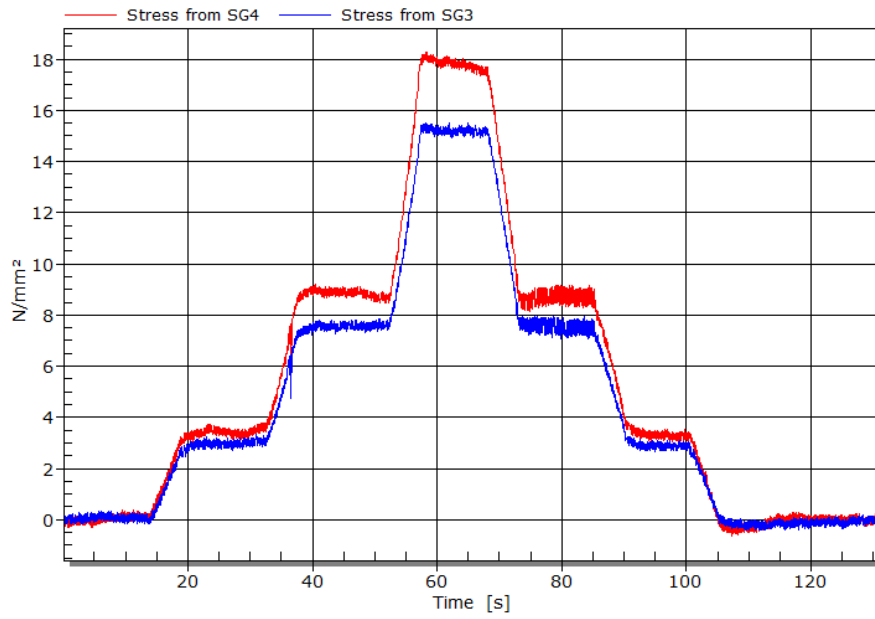


Figure E.14: Specimen 2 - Stress in strain gauge 3 and 4

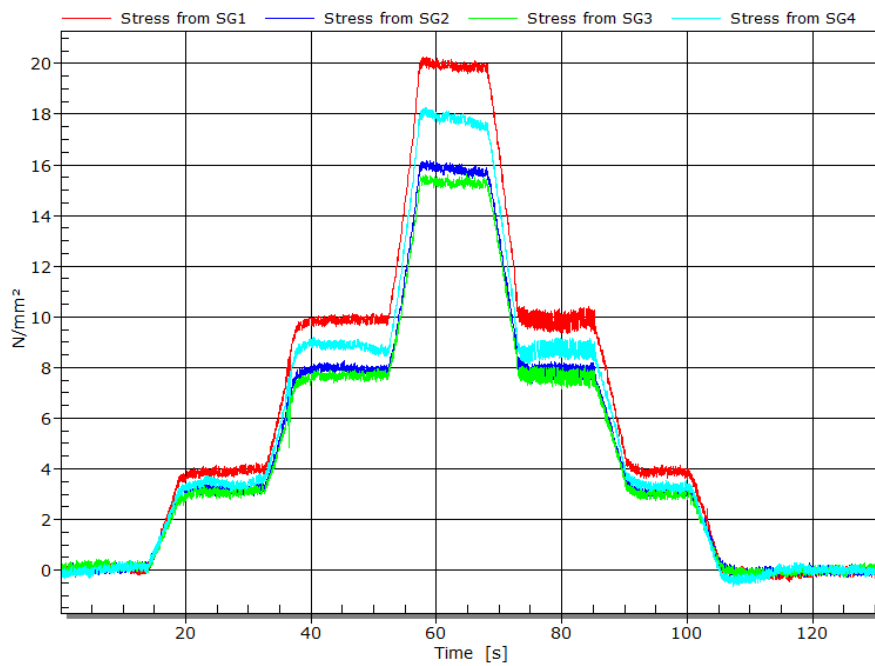


Figure E.15: Specimen 2 - Stress in strain gauge 1, 2, 3 and 4

